2020-01-01

Evaluation and Modeling of Electrodialysis for High-Recovery Brackish Water Desalination

Shahrouz Jafarzade Ghadimi
University of Texas at El Paso

EVALUATION AND MODELING OF ELECTRODIALYSIS FOR HIGH-RECOVERY BRACKISH WATER DESALINATION

SHAHROUZ JAFARZADE GHADIMI

Doctoral Program in Civil Engineering

APPROVED:

W. Shane Walker, Ph.D., Chair

Anthony J. Tarquin, Ph.D.

François Perreault, Ph.D.

Rafael Verduzco, Ph.D.

Stephen Crites, Ph.D.
Dean of the Graduate School

Dedication

I dedicate this work to my beloved parents, Abbas and Esmat, who are my source of inspiration, strength, and for their unconditional love and support throughout my life. Lord, thank you for them!

EVALUATION AND MODELING OF ELECTRODIALYSIS FOR HIGH-RECOVERY BRACKISH WATER DESALINATION

by

SHAHROUZ JAFARZADE GHADIMI, MSc

DISSERTATION

Presented to the Faculty of the Graduate School of

The University of Texas at El Paso

in Partial Fulfillment

of the Requirements

for the Degree of

DOCTOR OF PHILOSOPHY

Department of Civil Engineering

THE UNIVERSITY OF TEXAS AT EL PASO

August 2020

Acknowledgements

Performing research in the higher education setting is a life-changing opportunity. I hope this research mitigates the water scarcity by improving the understanding and practicality of water desalination. None of this could have happened without the support of my mentor and advisor, Dr. Shane Walker, who believed in me through thick or thin and provided his knowledge, insight, and mentorship. I deeply appreciate your friendship and brotherhood, and thankful for God's plan to know you and looking forward to more exciting projects. I do appreciate my Dissertation Committee, Dr. Anthony Tarquin, Dr. François Perreault, and Dr. Rafael Verduzco for their support throughout this study.

I am grateful to the staff and members of The University of Texas at El Paso. Special thanks to Dr. Malynda Cappelle, who shared her experience, knowledge, and excitement to make a difference in the water industry. My true appreciation to my friends and colleagues in the water quality lab, for their assistance through the experiments and analysis. I would thank all my colleagues and friends especially Martha Gonzalez, Julio Gallegos, and Jose Gutierrez for being willing to help selflessly. Thanks to my colleagues in the lab including Andres Sanchez, Avianna Gallegos, Daniela Hernandez, Denise Garcia, Eva Deemer, Francisco Solis, Frida Murga, Gabriela Porras, Golam Hyder, Juan Canales, Katie Lee, Mackayla Thyfault, Miguel Fraga, Tallen Capt, and Troy Svede for your company, enjoyment, and support during my time in the lab. Thank you Dr. Oluwaseye Owoseni, for your endless wisdom and brotherhood. You are a source of inspiration and I am proud to have you as a friend.

I do thank the Nanotechnology Enabled Water Treatment (NEWT) center supported by NSF, for their financial support, opportunity to collaborate with other researchers and colleagues from Rice, ASU, and Yale universities. It is a privilege to be a part of this center and see the actual

breakthroughs across inter-institutional collaborations. I do appreciate my colleague and brother, Dr. Douglas Rice from ASU under the supervision of Dr. François Perreault for the opportunity to collaborate on a research paper and leverage the acquired skills during this time.

I appreciate the help and cooperation of El Paso Water staff during this study, especially Art Ruiz, the Superintendent of the Kay Bailey Hutchison Desalination Plant, El Paso, TX. Thank you for your patience, understanding, and giving us the opportunity to perform experiments over a course of a year in the plant. My gratitude goes to Charlie He, P.E. from Carollo Engineers in Phoenix, AZ who mentored me during my internship program. Your support, knowledge, and wisdom prepared me for the next chapter of my life, and I genuinely appreciate it. I should thank my colleagues, mentors, and friends in the Phoenix office who welcomed me, taught me, and made me a part of their family. I do appreciate Randy Shaw, the facility manager of the Brackish Groundwater National Desalination Research Facility at Alamogordo, NM for his support and providing the opportunity to perform pilot testing with brackish water. Thanks to the engineers at Magna Imperio Systems for their innovation and helpfulness. Working with you made a huge difference in understanding the issues and new solutions of the water industry.

Thanks to my immediate family, who were by my side from the very first day. I never forget your relentless sacrifices and care to make sure that I can reach my goals. Thanks to my father who is my role model and has always been there for me. Thanks to mom for teaching me to be kind and caring toward others. Thanks to my sister, Shokoufeh, for being a source of excitement and joy.

In the end, thank you, Lord, for orchestrating my life and putting several pieces together to make my life more meaningful and lead me to help others.

Abstract

This research investigates the feasibility of desalination of brackish water with electrodialysis (ED), using laboratory testing and mathematical modeling. Several experiments were performed to characterize ion-specific transport and to evaluate tradeoffs between salinity removal and specific energy consumption. A 200 cm^2 Ameridia ED stack was used to perform desalination experiments with real brackish groundwater from the Kay Bailey Hutchison desalination plant in El Paso, Texas, and the results showed limiting current density of 160 A/m^2 for 5 cm/s. A higher conductivity reduction was observed for flow velocity of 5 cm/s compared to 13 cm/s. Ion transport selectivity (based on relative removal ratio) decreased in the order of Ca^{2+}, Cl^-, Na^+, and SO_4^{2-}. The electrical conductivity of multi-component aqueous solutions was modeled based on ionic composition and ion pair complexes. Several experiments were performed to calibrate the model and compare it with conductivity and cation transport number data cited in the literature. The developed model is capable of estimating the electrical conductivity and ionic transport numbers of aqueous solutions up to 100 mS/cm at 25°C with a root mean square error of 0.305 mS/cm, a relative root mean square error of 9.7%, and R-squared value of 0.997. A mathematical model for steady-state ED operation was developed based on Nernst-Planck ionic transport and other theoretical principals to simulate the hydraulic, chemical, and electrical performance of the system. The model accurately predicted the removal of sodium and chloride (R-squared of more than 0.96); however, the model significantly underpredicted calcium separation and overpredicted sulfate separation. The model predicted the SEC of low and high velocities precisely predicted with RRMSE of 8% and 18%, respectively. Future work should incorporate membrane selectivity into the transport modeling.

Keywords: Electrodialysis, Desalination, Mathematical Modeling

Table of Contents

List of Tables

List of Figures

Abbreviations

AEM:	Anion Exchange Membrane
BGNDRF:	Brackish Groundwater National Desalination Research Facility, Alamogordo, NM
CEM:	Cation Exchange Membranes
CRC:	CRC Handbook of Chemistry and Physics
DSE:	Dimensionally Stable Electrode
EC:	Electrical Conductivity
ED:	Electrodialysis
EPDM:	Ethylene Propylene Diene Monomer
HC:	High Concentration
IC:	Ion Chromatography
IEM:	Ion Exchange Membrane
KBH:	Kay Bailey Hutchison desalination plant, El Paso, TX
LC:	Low Concentration
LCD:	Limiting Current Density
NHE:	Normal Hydrogen Electrode
PP:	Polypropylene
PVC:	Polyvinyl Chloride
RMSE:	Root-Mean Squared Error
RRMSE:	Relative Root Mean Square Error
RO:	Reverse Osmosis
SEC:	Specific Energy Consumption
SS:	Stainless Steel
TDS:	Total Dissolved Solids

Mathematical Symbols

a:	Debye-Hückel parameter (Å)
b:	Debye-Hückel parameter
c:	Molar concentration (mol L^{-1})
c_1-c_7:	Constants function of temperature
d:	characteristic length or hydraulic diameter (m)
D:	Diffusivity (m^2 s^{-1})
E:	Total energy invested for a batch of desalinated water (kWh)
E:	Reduction potential (V)
E^0:	Standard reduction protentional (V)
F:	Faraday's constant (96,485 C eq^{-1})
h:	Thickness of the membrane in the direction of the flux (m)
i:	Current density (A m^{-2})
I:	Ionic strength (mol L^{-1})
J:	Molar flux (mol m^{-2} s^{-1})
K:	Convective mass transfer rate (m^2 s^{-1})
K:	Ionic product
k:	Mass transfer coefficient
MM:	Molar mass (g mol^{-1})
MV:	Molar volume of water (55.5 mol L^{-1} at 25 °C)
N:	Molar flow rate (mol s^{-1})
N_{cp}:	Number of cell pairs
P:	Power of the continuous flow desalination process (kW)
p:	pressure (Pa)
P_{mem}:	Permeability of the membrane
Q:	Volumetric flow (m^3h^{-1})
$\tilde{R}$:	Areal resistance (Ω m^2)
R:	Removal ratio
Re:	Reynolds No.
R_g:	Gas constant, 8.314 (J mol^{-1} K^{-1})
Sc:	Schmidt No
SEC:	Specific energy consumption (kWh m^{-3})
Sh:	Sherwood No.
t:	Transport number
T:	Temperature (K, °C, °F)
V:	Batch volume (m^3)
w:	Average distance between the electrodes (m)
w':	Root-charge weighted mass-fraction
X_1, X_2:	Conductivity fitting parameters
Y_1, Y_2, Y_3:	Solution density parameters (g cm^{-3})
z:	Ionic charge (including sign)
α:	ionic activity
α:	Modified transfer coefficient
β:	Complex coefficient
γ:	Activity coefficient
δ:	Diffusion boundary layer thickness (m)
$\varepsilon(T)$:	Dielectric constant of water at temperature T (F m^{-1})
ε:	Relative error of the mass balance
η:	Total overpotential (V)
κ:	Conductivity (mS cm^{-1})
λ:	Equivalent ionic conductivity (S m^2 eq^{-1}])
v:	kinematic viscosity (m^2 s^{-1})
v:	Superficial velocity in silt (m cm^{-1})
Π:	Osmotic pressure (Pa)
ρ:	Density of the solution (g cm^{-3})
Ψ:	Volume fraction of the solute in the solution
ϕ:	Electric potential (V)

Subscripts

0:	Infinite dilution
AEM:	Anion exchange membrane
anode:	Anode
bulk:	Bulk solution
c:	Concentrate
cathode:	Cathode
CME:	Cation exchange membrane
CO_2:	CO_2
Complex:	Charged complexes including two ions
cp:	Cell pair
d:	Diluate
DBL:	Diffusion boundary layer
diff:	Diffusion
ed:	Electrodialysis stack
electrodes:	Electrodes
equ:	Gas production equilibrium
F:	Feed
free:	Free ions
H^+:	Hydrogen (hydronium) ion
H_2:	Hydrogen gas
HC:	High concentration
i:	i^{th} species
jct:	Liquid junction potential
kin:	Kinematic electrical overpotential
LC:	Low concentration
lim:	Limiting
Mem:	Membrane surface
n:	n^{th} species
n-H^+:	First deprotonation
n-$2H^+$:	Second deprotonation
n-$3H^+$:	Third deprotonation
O_2:	Oxygen gas
osmosis:	Osmosis
res:	Resistance
rinse:	Electrode rinse solution
tot:	Total,
w, n:	n^{th} grid
w, n+1:	$n+1^{th}$ grid
W:	Water
zero:	Zero charged ions
κ:	Conductivity

Chapter 1. Steady-State Electrodialysis Experiments

1.1 Introduction

1.1.1 Background

The surface of Earth is covered with more than two times water than land, while less than one percent is considered freshwater [1]. Increasing population has led to an urgent need of using seawater and brackish water as alternatives to conventional drinking water supply [2]. Desalination technologies are a growing source of drinking water, and reverse osmosis (RO) has the highest desalination market share (60%-90%, depending on location) [3]. Other desalination technologies such as electrodialysis have different advantages and disadvantages, and in some cases can be more cost effective than RO.

Electrodialysis (ED) is a desalination technology that uses ion-selective (ion exchange) membranes and is driven by electricity to remove the charged ions from water. Like RO, ED has a much lower specific energy consumption than thermal desalination processes. ED can typically achieve greater hydraulic recovery than RO (especially when silica is the main limiting factor for RO recovery), is more tolerant of suspended solids in the feedwater than RO, and can employ continuous chlorination for biofouling control (which is not possible with conventional RO membranes). The very first industrial use of ED was implemented by Ionics in the mid-1950s, almost half a century after introducing ED concept by Maigrot and Sabates [4], [5]. Later, Ionics was purchased by GE, which recently sold the water division to Suez. In contrast to the RO market, which benefited from strong competition and standardization, technological innovation in the ED market has been slow, and the technology is not as mature as RO, which leaves significant opportunities for advancement. Figure 1.1 shows a schematic of ED process.

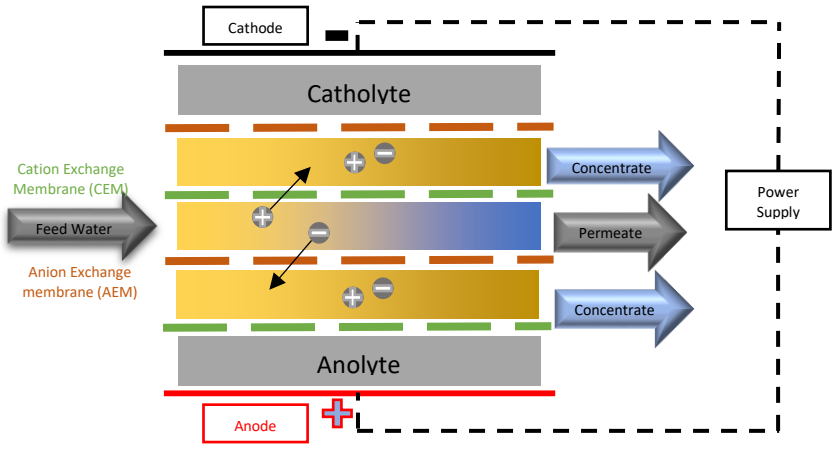

Figure 1.1: ED process schematic (adapted from [3])

This chapter discusses the feasibility of desalinating brackish water and RO rejection concentrate, using a laboratory-scale electrodialysis stack commercially manufactured ED system by Ameridia. Ameridia's system is a high-performance (higher recovery and lower energy) ED. This stack benefits from thinner membranes and spacers than Ionics/GE/Suez's ED stacks, which can decrease the overall energy consumption.

1.1.1.1 Goals and objectives

The overall goal of this research is to improve drinking water accessibility by improving desalination technology performance. The objectives of this research were to operate an ED system on real brackish and concentrate feedwater from the Kay Bailey Hutchison (KBH) desalination plant in El Paso, TX to characterize ion-specific transport and evaluate tradeoffs between salinity removal and specific energy consumption. Ultimately, the results of this chapter will be used for comparison with ED performance modeling in Chapter 3.

1.2 Methodology

The Kay Bailey Hutchison (KBH) Desalination Plant has a capacity of producing 27.5 million gallons per day of drinking water from brackish water and is located east of the El

Paso International Airport (El Paso, TX). At the time of testing (June 2020), the KBH brackish groundwater source had an electrical conductivity of 5.1 mS/cm. The major ionic composition of the solution is listed in Table 1.1.

Table 1.1: Concentrations of major ions for KBH brackish feed water (June 2020)

Ca^{2+} (mg/L)	K^{+} (mg/L)	Mg^{2+} (mg/L)	Na^{+} (mg/L)	Cl^{-} (mg/L)	F^{-} (mg/L)	SO_4^{2-} (mg/L)	NO_3^{-} (mg/L)	Alkalinity (mg/L as $CaCO_3$)
131	17.2	28.2	844	1399	1.0	419	N.D.[1]	80.6

[1] Not Detected

1.2.1 Experimental design summary

The performance of ED depends on operational parameters such as feed water conductivity, residence time, velocity, applied voltage, and current. A set of experiments was designed to study the effects of changes in feed velocity and stack voltage with respect to product water quality.

The experiments were performed at discrete values of applied stack voltage (ranging from 0.2 V/cell-pair to 2.0 V/cell-pair), two superficial velocities (5 cm/s and 13 cm/s), and feed water from KBH brackish groundwater with conductivity of 5.1 mS/cm.

1.2.2 Experimental system

The product and concentrate streams flow separately from 2-gal containers through the system. Electrode rinse was made from 99.9% pure sodium sulfate to make a 25 mS/cm solution. A BK Precision 9151 programmable DC power supply (< 20 V, < 27 A) was used as the power supply unit to apply voltage and current to the system. Two calibrated Thermo Scientific™ Orion Star ™ A329 meter with conductivity probes (013005MD) were used to measure conductivities for diluate and concentrate streams. The samples were analyzed with Thermo Scientific™ ion

chromatography (IC) simultaneous system (Dionex™ Aquion™ to analyze cations and Dionex™ Integrion™ HPIC™ system for analyzing anions).

The Ameridia stack (EUR2B-10) used in the experiments, which is made of stainless steel (SS) press plate (304), with electrode chamber and grid made of polyvinyl chloride (PVC). The anode and cathode electrodes are both dimensionally stable electrodes (DSE®). The stack consists of 10 Anion Exchange Membranes (AEM), and 11 Cation Exchange Membranes (CEM). The homogeneous membranes of ACS and CIMS produced by NEOSEPTA®-Astom Corporation were used as AEM and CEM, respectively [6]. The active surface area of membranes is 2 dm^2. The wet thickness of ACS and CMX are 130 µm and 175 µm [7], respectively. The wet exchange capacity of ACS and CMX are 2.0 meq/g [8] and 1.65 meq/g [9], respectively. The apparent counterion transport numbers for ACS and CMX are 0.98 [10], and 0.965 [11], respectively. The resistance of ACS and CMX for a 0.5 M NaCl solution is 3.8 Ω cm^2 [12] and 3.3 Ω cm^2 [12], respectively. The operation temperature for these membranes should be less than 45 °C (123 °F), while avoiding exposure too oxidizing agents (*e.g.*, hypochlorite), and organic solvents (*e.g.*, benzene and toluene). The gaskets are made from ethylene propylene diene monomer (EPDM), and spacer mesh and distributors are made from polypropylene (PP) with spacer dimensions of 11.4 cm×17.5 cm×0.08 cm. The volume and area porosity of spacer is 0.78 and 0.39, respectively. Figure 1.2 illustrates schematic diagram of Ameridia ED stack.

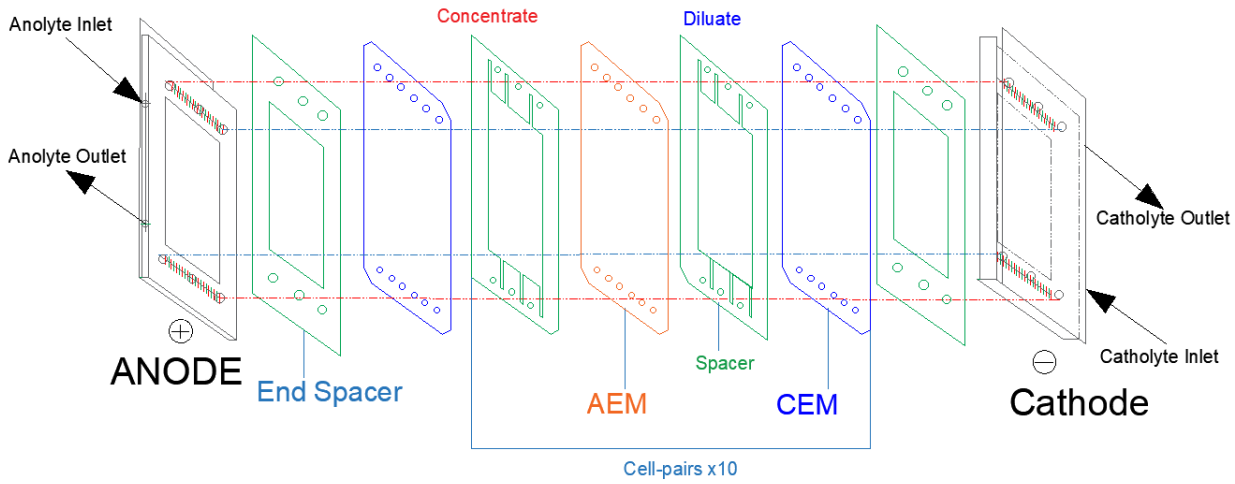

Figure 1.2: Ameridia ED stack schematic (adapted from Ameridia EUR2B-10 instruction manual)

To desalinate water with the stack, it is recommended to set the product flow rate, and the pressure in concentrate stream matches to the pressure in product stream. Three separate pumps were used to circulate solutions for each stream of product, concentrate and electrolyte (anolyte and catholyte).

Several tests were performed to characterize electrical operational limitations of the system. These tests included electrode voltage loss and limiting current density (LCD) for different flowrates, as explained below.

1.2.2.1 Electrode Voltage loss

The applied voltage to the stacks is not entirely being used for electrodialysis due to thermodynamic and kinetic voltage losses that occur at the electrodes. In other words, the net voltage that the membrane stack receives is equal to the difference of applied voltage and voltage loss at the electrodes. The voltage loss at the electrodes $\Delta\emptyset_{electrodes}$ can be approximated as [13]:

Equation 1.1

$$\Delta\emptyset_{electrodes} = \Delta\emptyset_{equ} + \Delta\emptyset_{kin} + \Delta\emptyset_{rinse}$$

where $\Delta\emptyset_{equ}$ is the voltage drop to maintain oxygen and hydrogen gas production equilibrium at anode and cathode, respectively, $\Delta\emptyset_{kin}$ is the kinetic electrical overpotential due to gas production at the electrodes, and $\Delta\emptyset_{rinse}$ is the restive voltage loss corresponding to the electrode rinse solution.

The stacks are operating as an electric cell that redox reactions occur at the surface of cathode and anode by an external power source. Oxidation of water to oxygen occurs at the anode, which produces oxygen gas, protons, and electrons, as shown in Equation 1.2.

Equation 1.2 $$2H_2O \Leftrightarrow O_2 + 4H^+ + 4e^-$$

where the standard reduction protentional (E^0) of this reaction is equal to 1.229 V vs. Normal Hydrogen Electron (NHE). The reduction potential of the anode (E_{anode}) at non-standard conditions is calculated by:

Equation 1.3 $$E_{anode} = E^0 - \frac{R_g T}{4F} ln\left(\frac{\{H_2O\}^2}{p_{O_2} 10^{-4pH}}\right)$$

where R_g is the gas constant (8.314 $\frac{J}{mol \cdot K}$), T is the temperature in kelvin (K), F is Faraday constant (96485.3 $\frac{C}{mol}$), $\{H_2O\}$ is the activity of water, pH is the negative logarithm of the activity of hydronium, and p_{O_2} is the partial pressure of oxygen gas at the anode.

The reduction of water to hydrogen gas occurs at the cathode:

Equation 1.4 $$2H_2O + 2e^- \Leftrightarrow H_2 + 2OH^-$$

where the standard reduction protentional (E^0) of this reaction is equal to -0.828 V vs. Normal Hydrogen Electron (NHE). The reduction potential of cathode ($E_{cathode}$) is calculated by:

Equation 1.5 $$E_{cathode} = E^0 - \frac{R_g T}{2F} ln\left(\frac{p_{H_2} 10^{-2\{pK_w - pH\}}}{\{H_2O\}^2}\right)$$

where p_{H_2} is the atmospheric pressure of hydrogen gas, and pK_w is the negative logarithm of the ionic product of water. The sum of these voltage drops equals to:

Equation 1.6 $$\Delta \emptyset_{equ} = E_{anode} - E_{cathode}$$

This thermodynamic minimal electrical potential to maintain gas equilibrium at both electrodes (at a pH of 7 at both electrodes) is approximately equal to 1.23 V.

Additionally, to maintain the heterogenous gas production at a certain rate, the surface overpotential can be estimated by a Tafel semi-empirical approximation as below [14], [15]:

Equation 1.7 $$\eta = \frac{R_g T}{\alpha F} - ln\left(\frac{i}{i_0}\right)$$

where α is the modified transfer coefficient, i is the current density, and i_0 is the exchange current density. The sum of these overpotentials at anode and cathode results in kinetic overpotential loss as below:

Equation 1.8 $$\Delta \emptyset_{kin} = \eta_{cathode} + \eta_{anode} = \eta_{total}$$

The total overpotential (η_{total}) was modeled with Equation 1.7.

The last voltage drop belongs to resistance caused by the electrode rinse solution that can be calculated by:

Equation 1.9 $$\Delta \emptyset_{rinse} = i \frac{w}{\kappa_{rinse}}$$

where i is the current density, w is the average distance between the electrodes, and κ_{rinse} is the conductivity of the electrode rinse solution.

The hydraulic fittings of the stack did not allow for performing voltage loss experiments, so the result from an experiment with a similar stack was used. Experiments were performed and modeled with an ED stack with active membrane area of 320 cm^2, and electrolyte solution of 5 mS/cm (which results in higher electrode voltage loss than the current experiments). These experiments were performed by setting a stack with only anode and cathode electrodes and a cation exchange membrane, without using concentrate and diluate spacers. By minimizing the sum of

squared errors, the values of α, i_0, and w for lower superficial velocity of 1.5 cm/s were simultaneously determined to be 0.15, 0.024 A m^{-2}, and 15 mm, whereas the higher velocity of 2.5 cm/s were 0.15, 0.028 A m^{-2}, and 14 mm, respectively. The results of the voltage drop modeling are compared to experimental measurements in Figure 1.3, which reveals that the electrode voltage loss for the two different flow rate setpoints is very close.

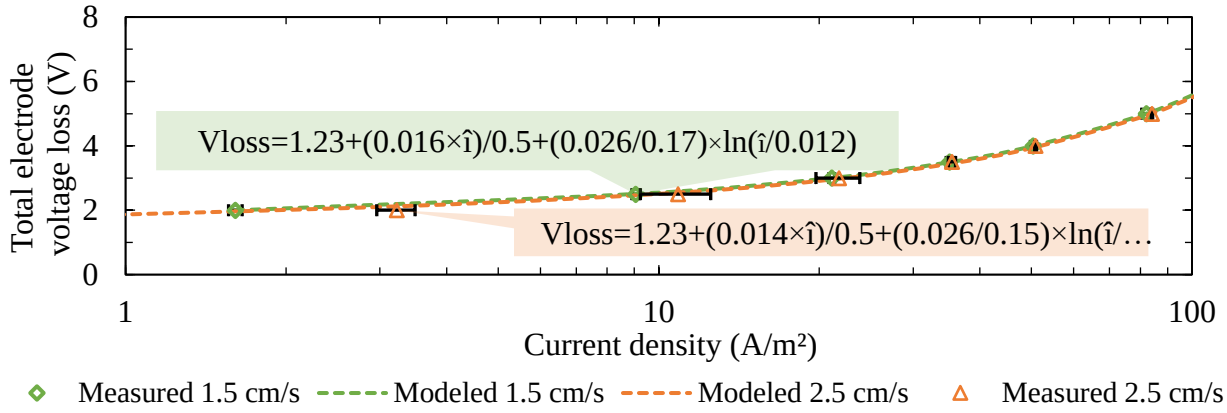

Figure 1.3: Measured and modeled voltage drop versus current density (Experiments were performed in triplicate at each flow rate.)

1.2.2.2 Limiting current density (LCD)

The current density through the electrodialysis stack increases with increasing voltage, which increases the concentration gradient in the diffusion boundary layer. The upper limit of current density occurs with approaching complete depletion of ions in the diluate diffusion boundary layer, as shown in Figure 1.4. This phenomenon defines the maximum current density in an electrodialysis stack and can be expressed as:

Equation 1.10

$$i_{lim} = \frac{F|z|C_D}{\bar{t}-t}\frac{D}{\delta} = \frac{F|z|C_D}{\bar{t}-t}k$$

where i_{lim} is the limiting current density (A m^{-2}), F is Faraday constant (96485.3 C/eq), z is ionic charge, δ is thickness of diffusion boundary layer (m), C_D is the concentration of diluate (mol/L), $\bar{t}$ and t are transport numbers of membrane and solution phases, respectively, D is diffusivity, and k is the mass transfer coefficient (which is the ratio of diffusivity over the thickness of the diffusion

boundary layer). As Ben et al. discussed, LCD depends on membrane solution conductivity, stack construction, and diluate velocity [16], [17]. There are empirical methods that can be used to determine LCD such as the Cowan-Brown and "shoulder" methods [18], [19]. As shown in Figure 1.4 (a), the current density is plotted against stack voltage per cell pair (after subtracting the electrode voltage loss), and the LCD is determined as the "shoulder" (*i.e.*, the intersection of two slopes). With the Cowan-Brown method shown in Figure 1.4 (b), area-specific resistance (Ω cm^2) is plotted against the reciprocal of current density (m^2/A), and the LCD is identified as the nadir of the curve. The two methods generally agree, but the Cowan-Brown method can be more precise in visualizing the LCD (*e.g.*, current densities of 160 A/m^2 for velocity of 5 cm/s). For higher velocity of 13 cm/s, the LCD was not identified, which means the stack can operate safely in this range. The results illustrate that for a given stack voltage (2.0 V/cell-pair), greater diluate velocity supports greater current densities.

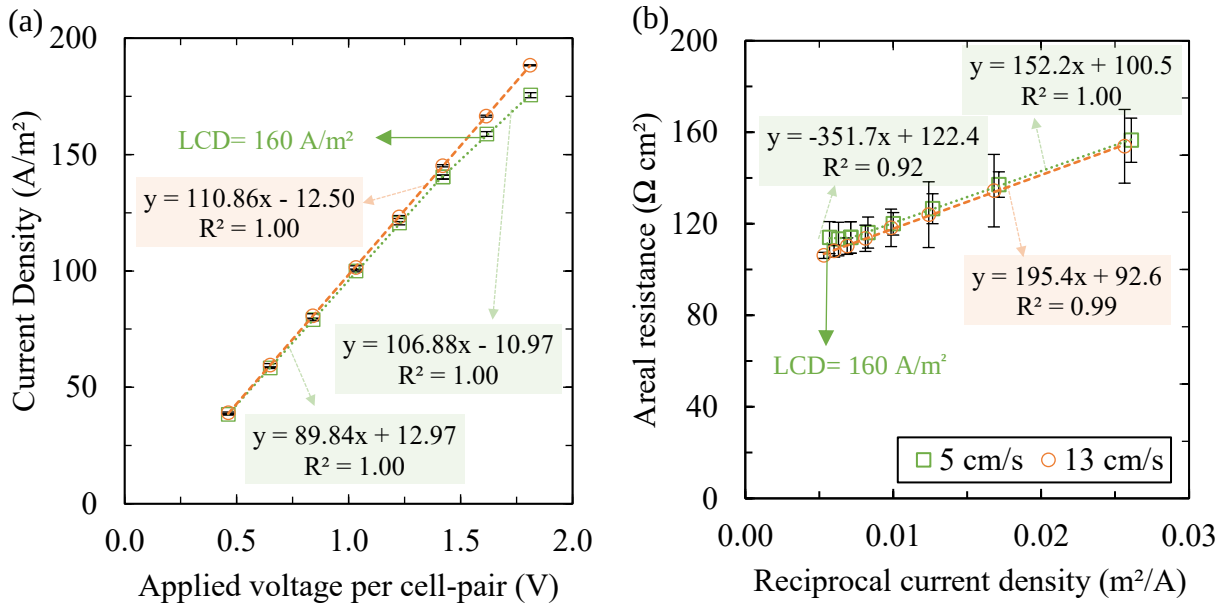

Figure 1.4: LCD measurement three replicates (n=3) for different flow velocities of 5 cm/s and 13 cm/s with (a) shoulder method, and (b) Cowan-Brown method

1.2.3 Desalination performance metrics

The desalination performance with ED is characterized by chemical, hydraulic, and electrical efficiencies which are explained below:

1.2.3.1 Salinity removal and conductivity reduction

The primary figure of merit for desalination processes is the concentration of salt (*e.g.*, total dissolved solids (TDS) or individual ions) that is removed from a solution. The formula for salt removal ratio is:

Equation 1.11 $$R = 1 - \frac{C_D}{C_F}$$

where C_D is the concentration of the diluate stream and C_F is the concentration of the feed. For simplicity, salinity removal can be approximated by conductivity reduction:

Equation 1.12 $$R_\kappa = 1 - \frac{\kappa_D}{\kappa_F}$$

where κ_D is the concentration of the diluate stream and κ_F is the concentration of the feed.

1.2.3.2 Specific Energy Consumption (SEC)

The Specific Energy Consumption (SEC) is the ratio of invested energy per unit volume of produced water:

Equation 1.13 $$SEC = \frac{E}{V_D} = \frac{P}{Q_D}$$

where SEC is the Specific Energy Consumption (kWh/m^3), E is the total energy invested for a batch of desalinated water (kWh), V_D is the batch volume of produced water (m^3), P is the power of the continuous flow desalination process (kW), and Q_D is the volumetric flow of desalinated water (m^3/h). The normalized SEC is the ratio of SEC per decrease in conductivity and is beneficial to compare the overall desalination performance regarding different product water set points:

Equation 1.14 $$SEC_{norm} = \frac{SEC}{\kappa_F - \kappa_D}$$

where SEC_{norm} is the normalized SEC with respect to conductivity (kWh m^{-3} mS^{-1} cm), κ_F is the feed water conductivity (mS/cm) and κ_D is the desalinated water conductivity (mS/cm).

1.3 Results and discussions

The results of measured outlet conductivities relative to conductivity of two different feed solutions for two flow velocities, and voltage are shown in Figure 1.5. (Concentrate and diluate flow rates were nearly identical, thus, experiments were performed at a nominal recovery of 50%.) As expected, greater single-pass steady-state separation is observed for flow velocity of 5 cm/s compared to higher velocity of 13 cm/s. The conductivity reduction ratio increased linearly with voltage application for slow and fast flow rates (5 cm/s and 13 cm/s), as shown in Figure 1.5 (b).

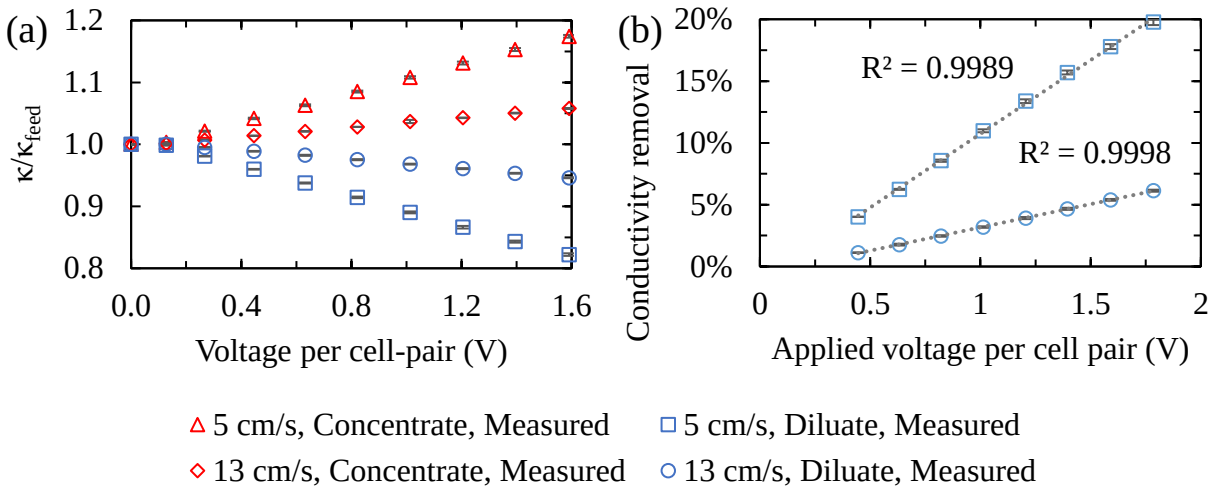

Figure 1.5: (a) Measured relative conductivity for diluate and concentrate outlets at different currents, flow velocities, for feed concentrations of 5.1 mS/cm, and (b) Relative conductivity reduction for single-pass steady-state ED

Similarly, the relative outlet concentrations of major ions are shown in Figure 1.6, versus applied voltage and flow velocity. Very consistent separation trends were observed for the 5.1 mS/cm feed, with decreasing selectivity in the following order: Ca^{2+}, Cl^{-}, Na^{+}, SO_4^{2-}.

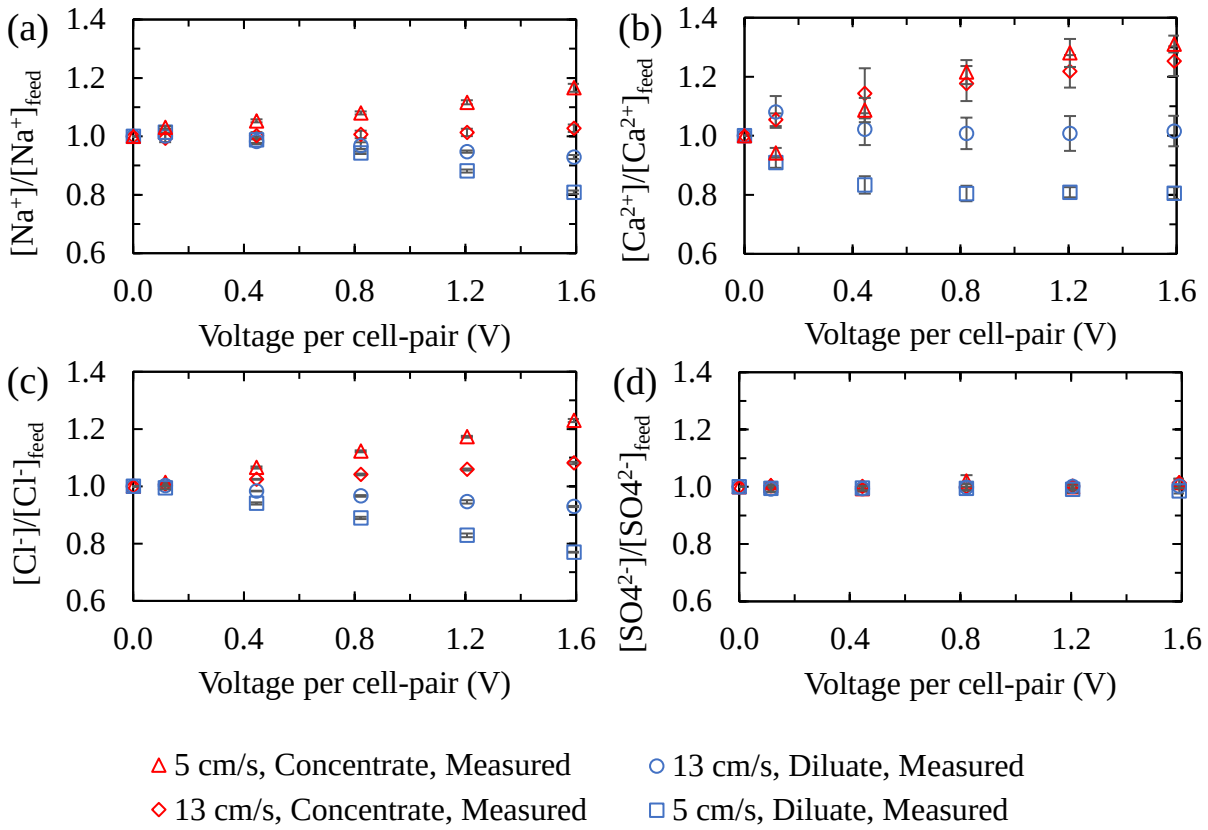

Figure 1.6: Measured relative concentrations for diluate and concentrate outlets at different voltage, flow velocity, in feed solution of 5.1 mS/cm for: (a) Sodium, (b) Calcium, (c) Chloride, and (d) Sulfate, respectively

The desalination SEC (*i.e.*, not including the hydraulic pumping power) is shown in Figure 1.7 (a). As it is shown, the slower flow rate needed more SEC than less faster flow rates. Figure 1.7 (b) compares the normalized desalination SEC which were the highest for faster flow rate than slower one.

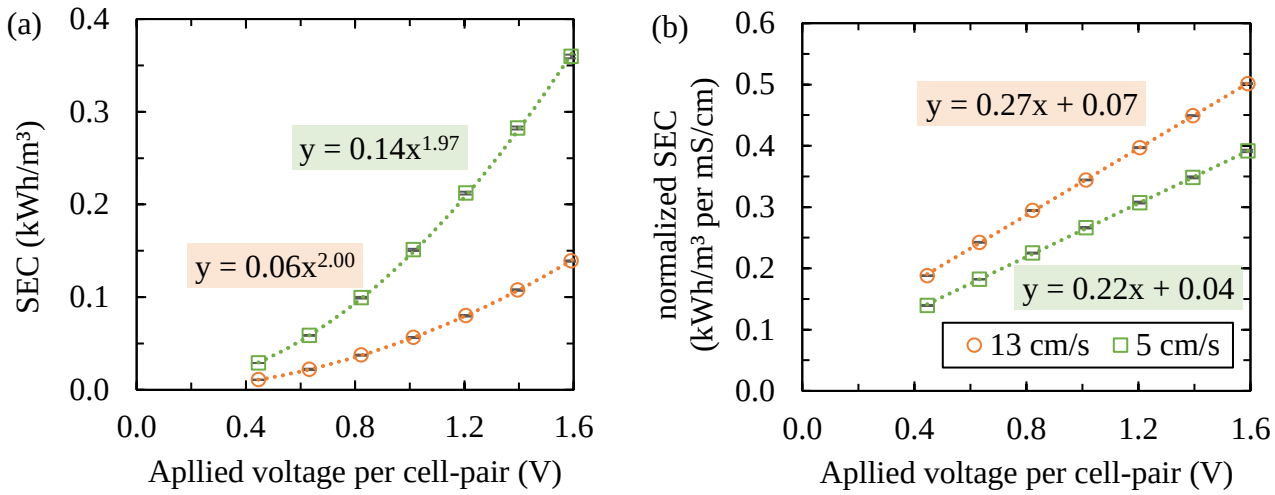

Figure 1.7: Desalination SEC and normalized desalination SEC for KBH feed (5.1 mS/cm)

1.4 Conclusions

An ED stack from Ameridia company was used to characterize ion-specific transport and evaluate tradeoffs between salinity removal and specific energy consumption. The stack consisted of 10-cell pairs of semi-permeable homogeneous membranes of CMX and ACS with an active cross-sectional area of 200 cm^2. The experiments were performed with a feed solution of brackish water from KBH (El Paso, TX) with a conductivity of 5.1 mS/cm. The water quality analysis indicated that the feed had a normality of 47.9 meq/L. The experiments were performed in triplicate for two flow velocities of 5 cm/s and 13 cm/s, with discrete applied voltage from 0.2 V/cell-pair up to 2.0 V/cell-pair.

The result of the experiments showed the LCD of 160 A/m^2 for velocity of 5 cm/s while an LCD was not detected (*i.e.*, greater than 190 A/m^2) for the higher velocity of 13 cm/s. As expected, the conductivity reduction of low flow velocity of 5 cm/s was higher than higher flow velocity of 13 cm/s, and conductivity reduction (*i.e.*, total salt removal) in the ED stack increased linearly with voltage application. The ion selectivity decreased in the order of Ca_2^+, Cl^-, Na^+, and

SO_4^{2-}. The SEC of slower flow velocity was more than faster flow velocity, whereas the normalized SEC has a reverse trend.

Future work should experiment with different feed solutions such as a RO concentrate with higher conductivities and different membranes to investigate the effects on conductivity reduction, ion selectivity, and SEC.

Chapter 2. Predicting Electrical Conductivity Based on Ionic Composition for Multi-Component Aqueous Solutions

2.1 Introduction

2.1.1 Background

Electrical conductivity (EC) is an intrinsic material property to convey electrical current. EC is often monitored as an indicator of the ionic content of an electrolyte or total dissolved solids (TDS) of aqueous solutions [1], [2] in industrial, environmental, and water treatment processes. Measuring conductivity is quick, easy, cheap, and accurate [1].

Modeling speciation in aqueous solutions was researched throughout the twentieth century [3], [4], and by the mid-1980s, with improvements in computational power, there were over 50 different programs developed to calculate the speciation and mass transport in aqueous solutions [4]. However, to date, very few models calculate EC, and for successful use in modeling electrically-driven separation processes such as electrodialysis and capacitive deionization, the model should calculate equivalent ionic conductivity (λ_i), transport number (t_i), and concentration (C_i) of each species (i) [20].

There do exist several models and software packages that predict conductivity based on ionic composition. For example, Standard Method 2510A [21] offers a simple mathematical expression to calculate conductivity based on concentration of ions, but it is not accurate for higher conductivity solutions. Software packages like WATEQ4F [22], Aqion, AqQa [23], and PHREEQCI [24] predict conductivity; however, they cannot be automatically called as a sub-routine in electrodialysis modeling.

2.1.2 Research goals and objectives

The goal of this research is to develop a model to calculate the electrical conductivity of an aqueous solution based on the concentrations of components and a basic set of complexation reactions among them. To achieve this goal, a mathematical model was developed based on fundamental principles and precisely calibrated with conductivity and transport number values obtained from literature. The model will be used as a sub-function to model electro-driven water treatment processes such as electrodialysis and capacitive deionization. The model was validated on synthetic and real brackish water solutions, as well as by comparison with other speciation software packages.

2.2 Methodology

2.2.1 Speciation

Depending on the source, environmental waters contain different concentrations of free ions, acids/bases, and complexes. Ions in the form of free ions or charged complexes contribute to overall ionic strength and the electrical conductivity of a solution. The process of calculating speciation and electrical conductivity is illustrated in Figure 2.1. First, the user enters total concentrations of each component. Second, the model calculates the ionic strength of the solution and then activity coefficients. Third, concentrations of free ions, acids and bases, and complexes are calculated. Fourth, the sum of all calculated species of each component are compared to the input total concentration, and the second and third steps are repeated until the relative error is less than 10^{-5} (0.001%). Finally, the electrical conductivity of the solution and transport number of each ion is calculated based on the speciation.

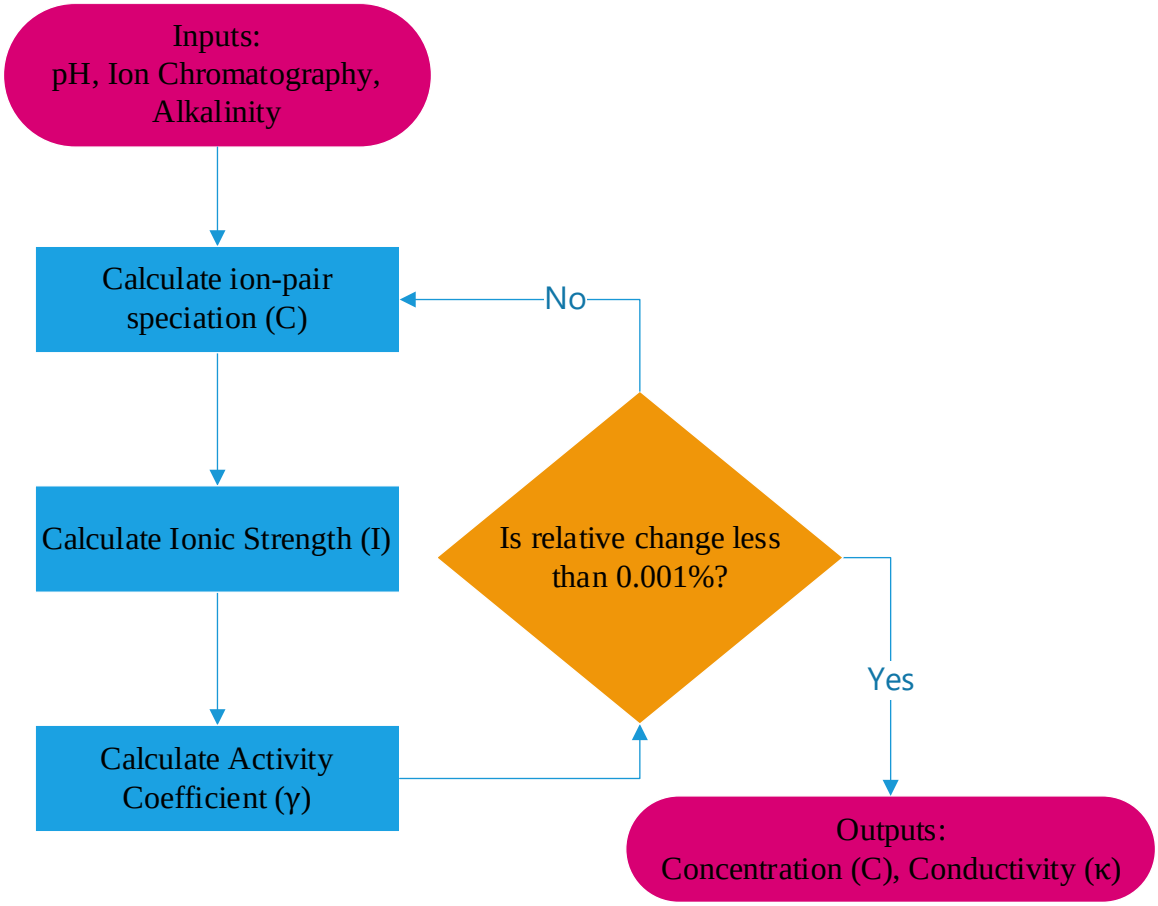

Figure 2.1: Flowchart of speciation and conductivity prediction model

Table 2.1 lists parameters used in the model such as molecular weight, charge, and å and b parameters of the Extended Debye-Hückel equation of the components.

Table 2.1: Molecular weight, charges, Extended Debye-Hückel parameters å, b, and diffusion coefficient at infinite dilution

Ions	MW (g/mol)	å (Å)	b (Å)	D_0 (10^{-5} cm^2/s)
H^+	1.01 [25]	9 [26]	0.015*	9.311 [27]
OH^-	17.01 [28]	3.5 [26]	-0.04**	5.273 [27]
Ba^{2+}	137.34 [28]	5 [26]	0.015*	0.847 [27]
Ca^{2+}	40.08 [28]	6 [26]	0.165 [28]	0.792 [27]
K^+	39.10 [28]	3 [26]	0.015 [28]	1.957 [27]
Mg^{2+}	24.31 [28]	6.5 [28]	0.2 [28]	0.706 [27]
Na^+	22.99 [28]	4 [26]	0.075 [28]	1.334 [27]
Sr^{2+}	87.62 [28]	5 [28]	0.015*	0.791 [27]
Br^-	79.90 [28]	4 [28]	-0.04**	2.080 [27]
Cl^-	35.45 [28]	3 [26]	0.015 [28]	2.032 [27]
F^-	19.00 [28]	3.5 [28]	-0.04**	1.475 [27]
NO^{3-}	62.01 [28]	3 [26]	-0.04**	1.902 [27]
SO_4^{2-}	96.06 [29]	5 [29]	-0.04 [29]	1.070 [24]

* Assumed equal to 0.015 for all cations such as K^+

** Assumed equal to -0.04 for all anions such as SO_4^{2-}

2.2.1.1 Activity coefficient and ionic strength

The activity of each species was calculated as the product of its activity coefficient and its concentration:

Equation 2.1 $$\alpha_i = \gamma_i \times C_i$$

where a_i is the activity of ith species, γ_i is the activity coefficient of that species, and c_i is the molar concentration of that ion. Several methods are available to calculate activity coefficients based on ionic strength. According to Wright [30], the Extended Debye-Hückel method is valid for solutions with ionic strength less than 1 mol/L and is shown in Equation 2.2 [30]:

Equation 2.2 $$\log(\gamma_i) = -Az_i^2\left(\frac{\sqrt{I}}{1+Ba_i^0\sqrt{I}}\right) + b_i I$$

where I is ionic strength (often reported in mol/L), $z_i$is the charge of ion i, a_i^0 (Ångström) and b_i are parameters related to each ion as listed in Appendix A, A and B are function of temperature, T (K), and dielectric constant which are calculated as below:

Equation 2.3 $$A = 1.82 \times 10^6 (\varepsilon(T) \times T)^{\frac{-3}{2}}$$

Equation 2.4 $$B = 50.29 (\varepsilon(T) \times T)^{\frac{-1}{2}}$$

Dielectric constant of water $\varepsilon(T)$ (F/m) in the range of 0°C to 100°C can be calculated as [31]:

Equation 2.5 $$\varepsilon(T) = [87.74 - 40T + 9.40 \times 10^{-4} T^2 - 1.41 \times 10^{-6} T^3] \mathrm{F/m}$$

where T is water temperature (°C). In a solution at 25°C, A= 0.511 $M^{-1/2}$ and B=0.33 $M^{-1/2} nm^{-1}$.

The Extended Debye-Hückel method was selected because it is more accurate than the Davies method (which does not account or differences among ions of the same charge) and less computationally intensive than the Pitzer method (which can be used for solutions up to 20 mol/L ionic strength [30]).

Calculation of the ionic strength of a solution is a function of ionic concentrations [32]:

Equation 2.6 $$I = \frac{1}{2} \sum_i c_i z_i^2$$

where I is the ionic strength, c_i is the concentration of ion i.

2.2.1.2 Hydrogen and hydroxide ions

The concentration of the hydrogen ion can be calculated based on the given pH, according to the following equalities:

Equation 2.7 $$pH = -log\{H^+\} = -log(\gamma_{H^+}[H^+])$$

where γ_{H^+} is the activity coefficient of the hydrogen ion, and $[H^+]$ is the concentration of the hydrogen ion (mol/L). Similarly, the concentration of the hydroxide ion can be calculated as:

Equation 2.8 $$[OH^-] = \frac{\frac{K_W}{\{H^+\}}}{\gamma_{OH^-}}$$

The pK_w for water at 25°C is 14.

2.2.1.3 Acids and bases

In this model, the equilibrium of acids and bases is calculated based on dissociation constants (pK_a) which are listed in Table 2.2.

Table 2.2: Acids and bases dissociation constant pK_a, charges, a, b, and diffusion coefficient D_0

Acids and base	pKa (mol/L)	MW (g/mol)	å (Å)	b	D_0 (10^{-5} cm^2/s)
$B(OH)_4^-$	9.31 [33]	78.839 [34]	3 [24]	-0.04*	1 [24]
HCO_3^-	6.35 [26]	61.017 [33]	3 [24]	-0.04*	1.185 [27]
CO_3^{2-}	10.33 [26]	60.009 [33]	4 [24]	-0.04*	0.923 [27]
$HSiO_3^-$	9.84 [26]	77.092 [34]	3 [24]	-0.04*	1.304 [24]
SiO_3^{2-}	13.20 [26]	76.084 [34]	4 [24]	-0.04*	1.015 [24]

* Assumed equal to -0.04 for all anions such as SO_4^{2-}

The concentration of acids were calculated as below [32]:

Equation 2.9
$$C_{f_{n-\mathrm{H}^+}} = C_{t_n}\left(\frac{\{H^+\}\gamma_{f_1}}{k_{a_1}\gamma_{f_0}} + 1 + \frac{k_{a_1}\gamma_{f_1}}{\{H^+\}\gamma_{f_2}} + \frac{k_{a_1}k_{a_2}\gamma_{f_1}}{\{H^+\}^2\gamma_{f_3}}\right)^{-1}$$

Equation 2.10
$$C_{f_{n-2\mathrm{H}^+}} = C_{t_n}\left(\frac{\{H^+\}^2\gamma_{f_2}}{k_{a_1}k_{a_2}\gamma_{f_0}} + \frac{\{H^+\}\gamma_{f_2}}{k_{a_2}\gamma_{f_1}} + 1 + \frac{k_{a_2}\gamma_{f_2}}{\{H^+\}\gamma_{f_3}}\right)^{-1}$$

Equation 2.11
$$C_{f_{n-3\mathrm{H}^+}} = C_{t_n}\left(\frac{\{H^+\}^3\gamma_{f_3}}{k_{a_1}k_{a_2}k_{a_3}\gamma_{f_0}} + \frac{\{H^+\}^2\gamma_{f_3}}{k_{a_1}k_{a_2}\gamma_{f_1}} + \frac{\{H^+\}\gamma_{f_3}}{k_{a_2}\gamma_{f_2}} + 1\right)^{-1}$$

where γ_{f_0} is the activity coefficient of zero charged species (*e.g.* $H_3PO_4^*$); $\gamma_{f_{CO_2}}$ is equal to $10^{0.1I}$[35]; $\gamma_{f_1}, \gamma_{f_2}, \gamma_{f_3}$ are the activity coefficients of the first, second, and third deprotonation of those species, respectively (*e.g.*, $H_2PO_4^-$, HPO_4^{2-}, and PO_4^{3-}, respectively), $k_{a_1}, k_{a_2}, k_{a_3}$ are the first, second, and third equilibrium constants, respectively, C_{t_n} is the total concentration of n^{th} component (*e.g.*, sum of all species derived from carbonate, bicarbonate, and carbonic acid), and $C_{f_{n-\mathrm{H}^+}}$, $C_{f_{n-2\mathrm{H}^+}}$, and $C_{f_{n-3\mathrm{H}^+}}$ are the first, second, and third deprotonations of that component, respectively (if they exist).

The activity of water was assumed as equal to mole fraction of water which was approximated as:

Equation 2.12 $$\{H_2O\} = 1 - \frac{C_{free}+C_{Complex}+C_{Zero}}{MV_w}$$

where MV_w is the molar volume of water, which is dependent on temperature and is equal to 55.5 mol/L at 25 °C.

2.2.1.4 Ion-pair complexes

The most abundant charged and neutral complexes were included based on Visual Minteq [33] software simulation to represent more than 99% of the species of each component for the simulated and real waters tested. The complexation constant (β) values are shown in Table 2.3 [33].

Table 2.3: Charged and neutral complexes and stability constants (log(β)) [33]

Complex	log(β) (L/mol)	Complex	log(β) (L/mol)
$BaCl^+$	-0.03	$MgCl^+$	0.60
$BaCO_3$	-9.24	$MgCO_3$	-9.20
$BaHCO_3^+$	0.98	MgF^+	1.90
$BaNO_3^+$	0.70	$MgHCO_3^+$	1.011
$BaSO_4$	-6.35	$MgSO_4$	-12.10
$CaB(OH)_4^+$	1.76	NaCl	-12.7
$CaCl^+$	0.40	$NaCO_3^-$	1.27
$CaCO_3$	-10.33	NaF	-2.30
CaF^+	1.14	$NaHCO_3$	-6.80
$CaHCO_3^+$	1.10	$NaNO_3$	-11.60
$CaNO_3^+$	0.50	$NaSO_4^-$	0.74
$CaSO_4$	-9.90	$SrCl^+$	0.19
KCl	-13.10	$SrCO_3$	-11.70
KSO_4^-	0.85	$SrHCO_3^+$	1.21
$MgB(OH)_4^+$	1.54	-	-

The concentration of ion-pair complexes and zero charged species are calculated based on stability constants and the activity coefficients of each species:

Equation 2.13 $$C_{complex_n} = \beta_{complex_n} C_{free_a} C_{free_b} \gamma_{f_a} \gamma_{f_b} \gamma_C^{-1}$$

where $C_{complex_n}$ is the concentration of the complex of two ions of "a" and "b" with equation constant of $\beta_{complex_n}$ and calculated γ_C from Equation 1.15. The activity coefficient of neutral (zero) charge complexes (γ_{zero}) is estimated as $10^{0.1I}$ [36].

2.2.1.5 Model convergence

Initially, the concentrations of free species are approximated as equal to their respective components. At the end of each iteration, the concentrations of free species are adjusted are:

Equation 2.14 $$C_{free_n} = C_{tot_n} - \frac{1}{1+\varepsilon}(C_{complex_n} + C_{zero_n})$$

where C_{free_n} is the concentration of the free species, C_{tot_n} is the input total concentration of species (*e.g.*, total carbonate), ε is the relative error of the mass balance of each respective component, , and $C_{complex_n}$ and C_{zero_n} are the concentration of ionic complexes and neutral ion pairs of the specified ion, respectively.

Iterations conclude when the maximum relative error of mass balance between the calculated and input concentrations is less than 10^{-5} of total concentration for each component.

2.2.2 Electrical Conductivity Model and Calibration

Modeling the electrical conductivity of multicomponent solutions is necessary as a function of composition because the overall conductivity is the result of the movement of ionic species in a solution. After speciation has been calculated, the conductivity of each sample can be calculated as the sum of conductivity of each constituent [14]:

Equation 2.15 $$\kappa = \sum_i \lambda_i C_i |z_i|$$

where κ is the conductivity of the solution, λ_i is the equivalent conductivity of each ion (subscript *i)*, C_i is the equivalent concentration of each ion, and $|z_i|$ is the absolute value of charge of each ion.

The equivalent ionic conductivity of each ion is calculated by multiplying the equivalent ionic conductivity at infinite dilution (λ_0) by the conductivity coefficient (γ_{λ_i}), which is analogous to the method of calculating activity:

Equation 2.16 $$\lambda_i = \lambda_{0_i}\gamma_{\lambda_i}$$

The equivalent ionic conductivity at infinite dilution (λ_{0_i}) is often reported in units of $\left(\frac{S\,cm^2}{eq}\right)$ and can be calculated based on ionic diffusivity [14]:

Equation 2.17 $$\lambda_{0_i} = \frac{F^2}{RT}|z|D_0$$

where, F is the Faraday constant equal to 96485 $\frac{C}{eq}$ at 25ºC, R is the universal gas constant equal to 8.314 J mol^{-1} K^{-1} at 25ºC, T is the temperature, $|z|$ is the absolute value of charge for each ion, and D_0 is the diffusivity at infinite dilution and has been included in Table 2.1 and Table 2.2.

A one-parameter expression for estimating the conductivity coefficient was inspired by the Debye-Hückel activity coefficient expression, and after multiple iterations and tests with various expressions, the following expression performed the best:

Equation 2.18 $$\gamma_{\lambda_i} = 10^{\frac{X_1|z|\sqrt{I}}{|z|+X_2 å\sqrt{I}}}$$

where I is the ionic strength, å is empirical number related to the size of the components in angstrom, and X_1 and X_2 are the model fitting parameters. These fitting parameters were determined based on 109 published conductivity values [27], [37] of several solutions with concentrations ranging from 0.5 mM to 1 M. Moreover, cation transference numbers (*i.e.*, the ratio of positive ion conductivity to the overall conductivity of a single salt solution) from Kortüm

[37] were compared for various species to constrain conductivity contributions from anions and cations. The best fitting values of X_1 and X_2 were -0.174 and 0.181, respectively, which minimized the root-mean squared error (RMSE) of 0.305 mS/cm and corresponded to a relative root mean square error (RRMSE) of 9.7% and an R-squared value of 0.9974. With these fitting parameters, the modeled conductivity values are compared against the literature reported values in Figure 2.2, and the equivalent ionic conductivity values are shown as a function of ionic strength in Figure 2.3. Modeled cation transport numbers (transference) are predicted well with a RRMSE of 3% and highly correlated with R^2 of 0.9855, compared against literature values, which are shown in Figure 2.4.

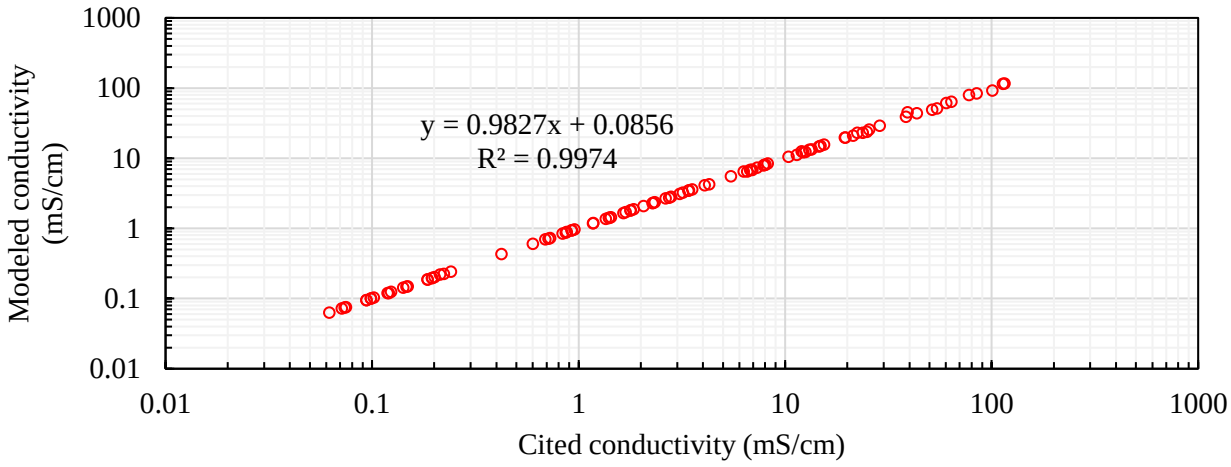

Figure 2.2: Comparison of modeled conductivity (κ) with literature conductivity values

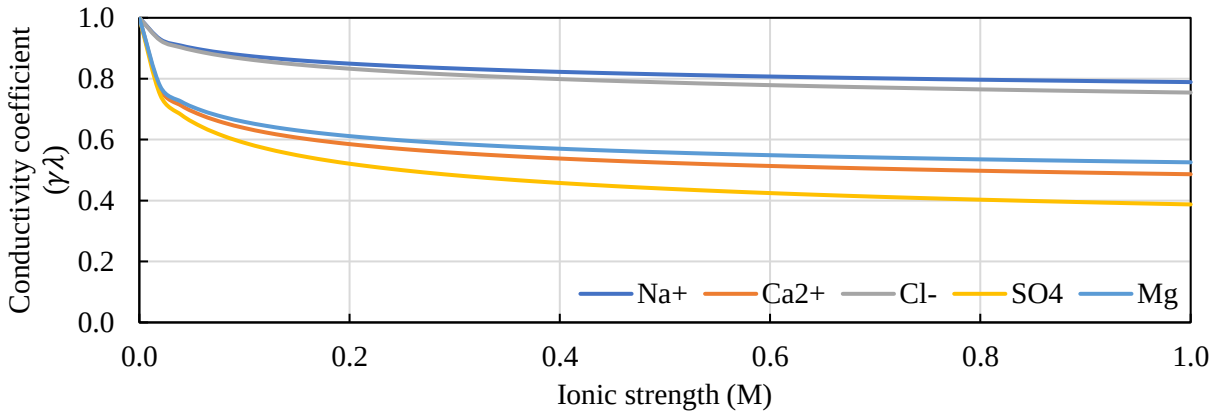

Figure 2.3: Modeled conductivity coefficient (γ_λ) versus ionic strength

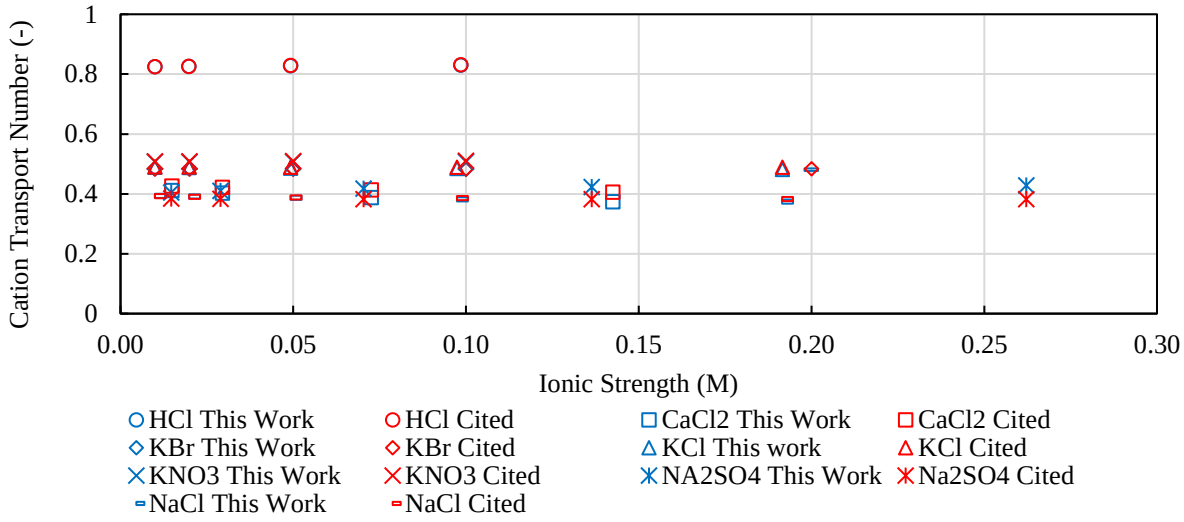

Figure 2.4: Cation transport number versus ionic strength (modeled and literature values)

2.3 Results and Discussion

The electrical conductivity model developed in this work was compared with reported conductivity values from literature [27], [37], as shown in Figure 2.5. Furthermore, the model developed in this work was compared with two other models for calculating electrical conductivity. For the calibration dataset, the EC model developed in this work had relative error less than ±10% for EC up to 100,000 µS/cm and was more accurate than the WATEQ4F model and the Standard Method 2510A (RRMSE values of 12%, 18%, and 25%, respectively).

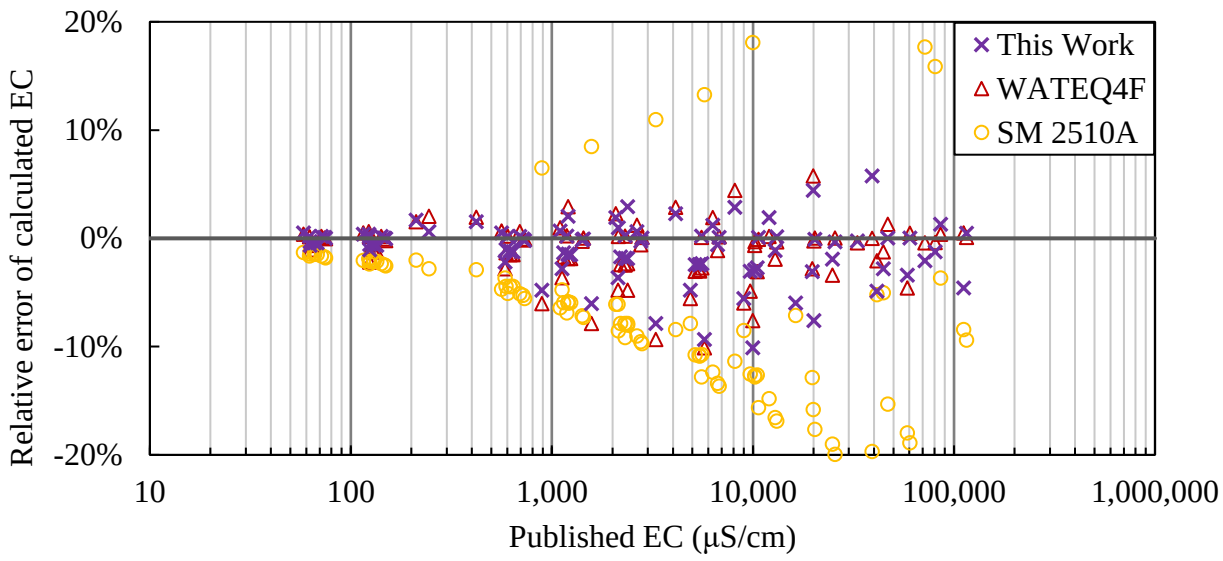

Figure 2.5: Relative error comparison this work (purple cross) and other methods vs. published EC

To further validate the model, multiple synthetic solutions were prepared with mass-balance precision of 0.01 mg for concentrations from 1 mN to 1 N. Several multi-component synthetic solutions were precisely prepared from five different solutes of $NaHCO_3$, Na_2SO_4, $MgSO_4$, NaCl, $CaCl_2$. The ratio of mixing these chemicals are demonstrated in Table 2.4:

Table 2.4: Ratio of each element and measured solutes to make 0.1N solutions

	Analyte	Mixtures			
		A	B	C	D
Cations (%)	Na^+	65%	85%	100%	100%
	Ca^{2+}	25%	10%	0%	0%
	Mg^{2+}	10%	5%	0%	0%
Anions (%)	Cl^-	65%	85%	30%	60%
	HCO_3^-	25%	10%	60%	0%
	$SO4^{2-}$	10%	5%	10%	40%
Solutes (mg/L)	$NaHCO_3$	1,010.65	1,010.65	5,041.54	-
	$MgSO_4$	10,500.25	10,500.25	-	-
	NaCl	3009.61	3,009.61	1,752.74	3,506.49
	$CaCl_2$	116,856.80	116,856.80	-	-
	Na_2SO_4	-	-	1,610.95	6,444.20

The samples were prepared in a half liter Pyrex volumetric flask with precision of 0.20 mL and mixed completely with a magnetic bar for half an hour. Afterwards, the solutions were kept in a plastic sample bottle in a Thermo Fisher Scientific water bath (Model 2870) at 25°C. A calibrated Thermo Fisher Scientific Orion A325 meter with pH probe (8107UWMMD) and conductivity probe (013005MD) was used to measure pH, conductivity, and temperature of the samples, maintaining all at 25°C (±0.1°C). Figure 2.6 shows the relative error of the EC model in this work for these synthetic solutions, as well as a comparison against two other models. All the models except standard methods predicted the electrical conductivity within 20% of measured conductivity.

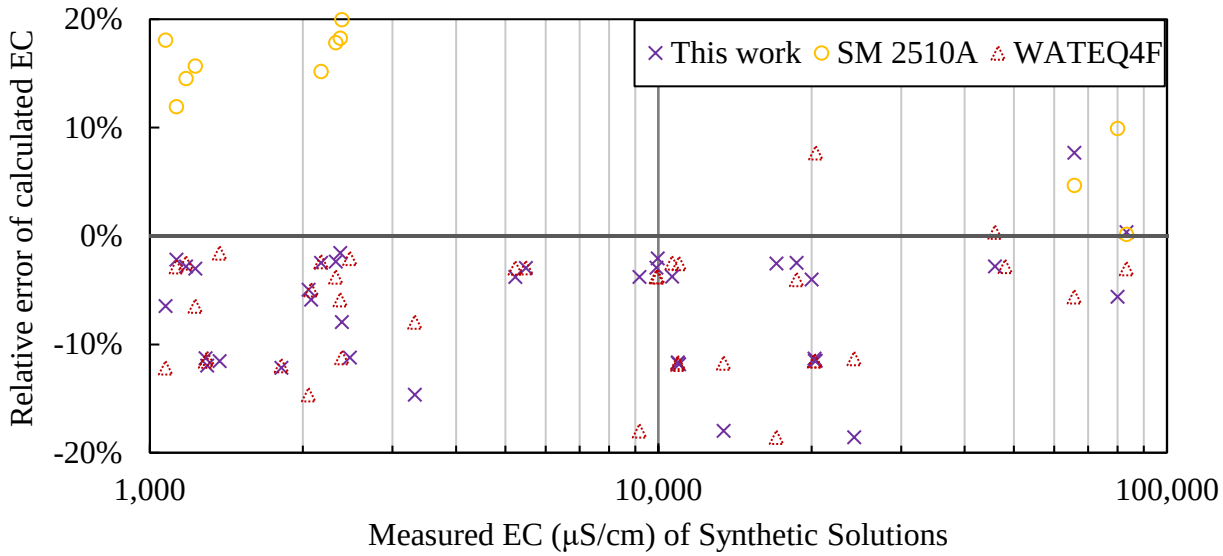

Figure 2.6: Relative error of calculated EC for synthetic solutions with this work and other methods versus measured EC

Finally, twenty-four real brackish water samples from the Brackish Groundwater National Desalination Research Facility (BGNDRF) in Alamogordo, NM were analyzed with the developed model to calculate EC. Figure 2.7 shows the result of running the model and comparison with other methods.

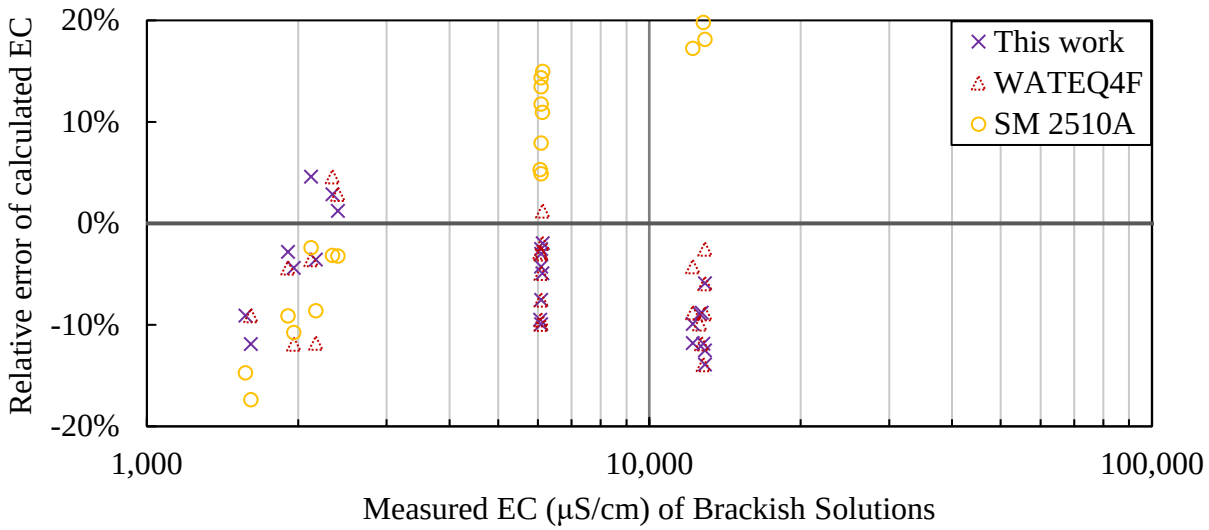

Figure 2.7: Relative error of calculated EC for brackish solutions with this work and other methods versus measured EC

2.4 Conclusions

A speciation and electrical conductivity model based on multi-component solutions was developed to accurately calculate the electrical conductivity and transport numbers of aqueous solutions up to 100,000 µS/cm at 25°C with relative errors of less than ±10%.

The calibration of the model with the cited solutions of 0.5 mM to 1 M concentration were performed accurately with a root mean square error (RMSE) of 0.305 mS/cm which corresponded to a relative RMSE of 9.7% and an R^2 of 0.9974. Validation of the model was performed with multi-component synthetic solutions ranging from 1 mN to 1 N with ±20% accuracy for solutions up to 100,000 µS/cm, which was more accurate than other methods. In the end, the model predicted 24 real brackish water solutions from the Brackish Groundwater National Desalination Research Facility (BGNDRF) in Alamogordo, NM within ±15%.

Future work should investigate the effects of expanding the complexity of the activity of water based on accounting for the density of the solution as a function of the composition. This

model will be utilized as a sub-routine in subsequent modeling in the design and optimization of electro-separation processes such as electrodialysis (ED) and capacitive deionization (CDI).

Chapter 3. Process Modelling of Electrodialysis

3.1 Introduction

3.1.1 Background

There have been several recent studies on fundamental and semi-empirical process modeling of ED [3], [17], [38]–[46]. Nikonenko et al. [45] reviewed multiple 2D and 3D mathematical models on ion-exchange membranes and electromembrane systems to discuss different membrane designs that can result in enhancement of ion transport in electrodialysis [45]. Campione et al. [3], performed an extensive literature review on theoretical, as well as experimental, characterization of the complex phenomenon occurring in electrodialysis and strategies to optimize the performance considering capabilities and limitations of each approach [3]. In another study, Campione et al. [46], developed a semi-empirical model for the ED process that requires membrane properties as input (*e.g.*, membrane resistance and salt and water permeability) to predict the performance of lab scaled ED for designing and optimization purposes [46].

These studies have improved the scientific understanding of ED operation based on theoretical and empirical modeling, but unfortunately, most of these models were developed based on binary solutions (*e.g.*, only sodium chloride), not multicomponent mixtures. To the best of our knowledge, there is no open source software (as opposed to commercially exclusive software packages such as Suez ED predictive software WATSYS) available for modeling the ED process.

3.1.1.1 Goals and objectives

The goal of this modeling is to improve access to drinking water by improving ED modeling, which will ultimately facilitate more efficient design and operation. The objectives of this chapter are to (1) create a mathematical model based on theoretical principals for

multicomponent solutions, and (2) calibrate and validate the model with the results from the first chapter of this dissertation.

3.2 Methodology

This section describes the methodology of modeling the chemical, hydraulic, and electrical performance of the ED system.

3.2.1 Model calibration with lab-scale experiments

Data acquired from lab-scale experiments which were explained in Chapter 1, are used to calibrate the model. These data included water quality (feed, product, concentrate), flow rates, applied voltage, and current density.

3.2.2 Steady-State Electrodialysis

Simulation of electrodialysis in steady-state operation is a function of space within the electrodialysis stack. This simulation is approximated as one-dimensional for hydraulic and electrical parameters such as flow rate and current density and two dimensional for chemical concentrations, as shown in Figure 3.1. The flow inside each cell is approximated with stagnant boundary layers adjacent to the membranes and constant flow between. Hence, electrical current and flow rate are constant along the x-dimension and change along y-dimension, while chemical concentrations are two-dimensional and vary along the flowpath and perpendicular to the membranes *(i.e.,* y- and x-dimensions, respectively).

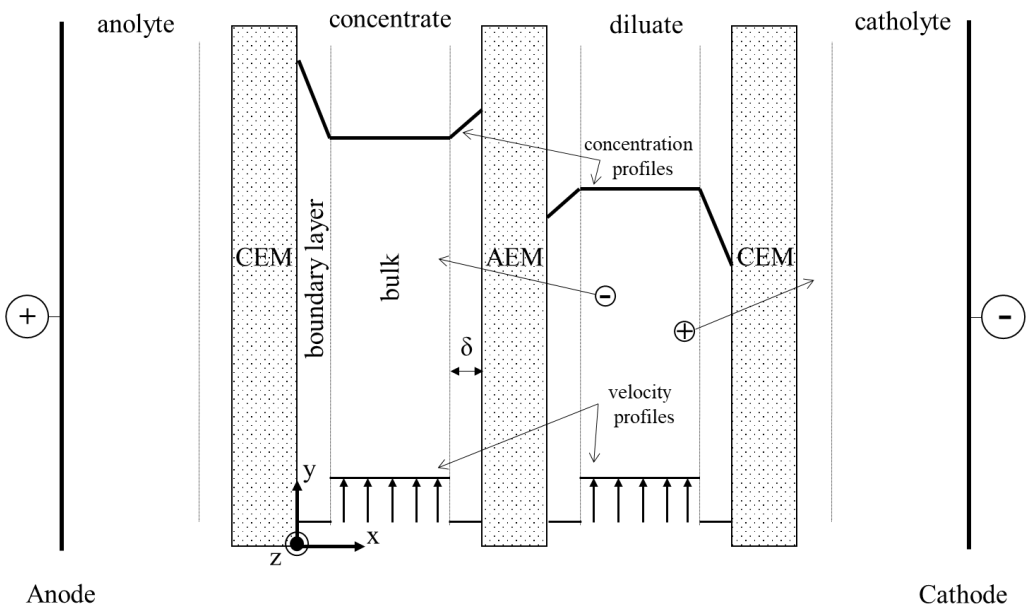

Figure 3.1: A single cell pair of an electrodialysis stack with velocity and concentration profiles - adapted from [47]

The electric behavior of the electrodialysis stack is modeled according to Ohm's law (multiple resistances in series) with the incorporation of multiple non-ohmic phenomena. The given parameters in the modeling are: feedwater component concentrations, ED stack geometry, spacer dimensions and properties, flow rate (velocity), total applied voltage, and IEM properties. The flow chart of modeling is shown in Figure 3.2 for each discretized distance along the flow path.

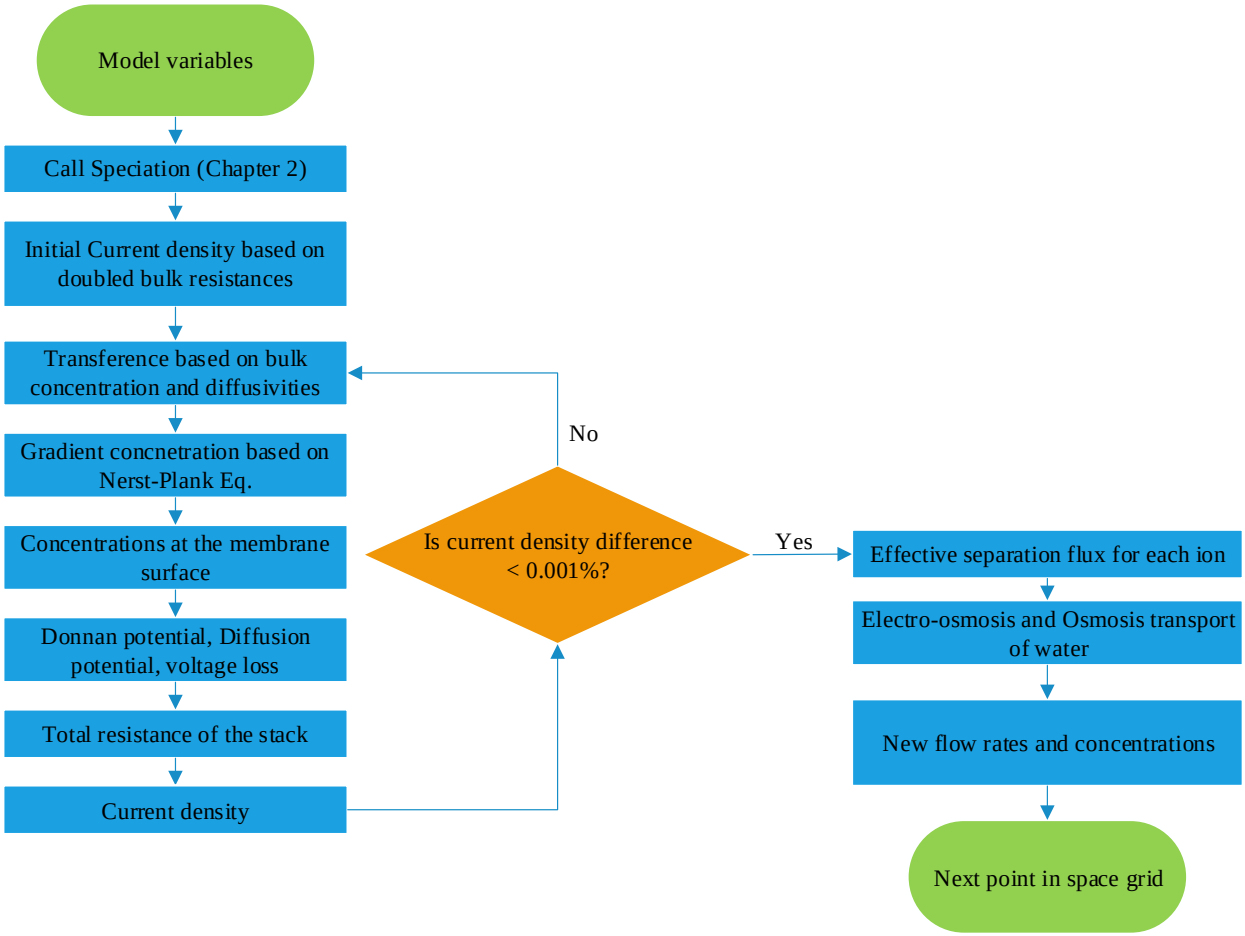

Figure 3.2: Flowchart of running the steady-state ED stack model

Each part of the mentioned flowchart is being explained in the following sections. The following assumptions were made based on Lee et al [48] while improving the modeling of an electrodialysis stack for hydraulic, chemical, and electrical parameters.

Hydraulic

- Concentrate and diluate cells have the same geometry but are allowed to have different flow rates.
- The diffusion boundary layer thickness is modeled as an empirical function of Reynolds number instead of being neglected entirely.

- Water transport through the membranes by electroosmosis and osmosis is incorporated instead of being neglected.

Chemical

- The electrical conductivity of the solution is a non-linear function of the multicomponent speciation (*i.e.*, Chapter 2) instead of being a linear function of a single binary salt (*e.g.*, NaCl).
- Activity coefficients are modeled as a function of the multicomponent solution [15]

3.2.3 Hydraulic Modeling

3.2.3.1 Diffusion boundary layer thickness

The diffusion boundary layer thickness (δ) has significant impacts on ionic separation in an ED system [15]. In recent studies by Chehayeb et al. [49]–[51], the diffusion boundary layer was determined by experimental correlation with the Sherwood Number (Sh) in which the mass transport was modeled based on Maxwell-Stefan approach [46]. The diffusion boundary layer thickness is calculated based on well-established fluid mechanics correlations as a function of Reynolds number [52]. One of these correlations is Sherwood No., which is the ratio of convective mass transfer rate over diffusion rate, which is a function of Reynolds and Schmidt number, and can be calculated as [52], [53]:

Equation 3.1

$$\frac{\mathrm{kd}}{D} = a\left(\frac{d\,v_{avg}}{\nu}\right)^{0.8-0.88}\left(\frac{\nu}{D}\right)^{0.25-0.33}$$

where $\frac{kd}{D}$ is the Sherwood No., $\frac{dv^0}{\nu}$ is Reynolds No., $\frac{\nu}{D}$ is Schmidt No., k is the convective mass transfer coefficient (m s^{-1}), D is mass diffusivity (m^2 s^{-1}), d is the characteristic length or hydraulic diameter (m), $v_{avg}$is the average superficial velocity in the slit (m/s), and ν is the kinematic viscosity (m^2 s^{-1}). The boundary layer thickness can be estimated as [53]:

Equation 3.2 $$\delta = \frac{D}{k}$$

3.2.3.2 Solution density

In order to precisely incorporate mass balance in the model, the density of a multicomponent solution (ρ) is described by a regression of mass-fraction for binary solutions. The following expression shows the solution density as a function of root charge-weighted solute mass fraction (w') within 1% accuracy [15]:

Equation 3.3 $$\rho = (0.7153\, w' + 0.9970)\, \frac{g}{cm^3}$$

The root-charge weighted mass-fraction (w') calculate as:

Equation 3.4 $$w' = \frac{\sum_i (c_i MM_i \sqrt{|z_i|})}{\rho}$$

where c_i is the concentration (mol/L) of species *i*, MM_i is the molar mass (g/mol), and z_i is the charge. Substitution of Equation 3.4 into Equation 3.3, can be simplified to:

Equation 3.5 $$\rho = \frac{1}{2}\left(Y_2 + \sqrt{{Y_2}^2 + \frac{4Y_1Y_3}{1000}}\right)$$

where Y_1= 0.7153 g/cm^3, Y_2= 0.9970 g/cm^3 (which is the density of pure water at 25°C), and Y_3=$\sum_i \left(c_i MM_i \sqrt{|z_i|}\right)$ in units of g/cm^3.

3.2.3.3 Electro-osmosis

Electro-osmosis is the flux of water with ions through the IEM. Table 3.1 shows the reported electro-osmosis numbers used in the model which are taken from hydration numbers reported in the literature [30], [54].

Table 3.1: Electro osmosis numbers (ionic hydration numbers)

Ion	Hydration	Ion	Hydration
Ba^{2+}	9	Br^-	4
Ca^{2+}	12.2	Cl^-	4
K^+	3	HCO_3^-	6
Mg^{2+}	14	NO_3^-	6
Na^+	5	SO_4^{2-}	6
Sr^{2+}	10.8	-	-

3.2.3.4 Osmosis

Osmosis refers to the flux of water molecules through IEMs from the side with lower salt concentration to the side with higher salt concentration:

Equation 3.6
$$J_{osmosis} = \frac{P_{mem}\Delta\Pi_{avg}}{h_{mem}}$$

where P_{mem} is the permeability of the membrane, h_{mem} is the thickness of the membrane in the direction of the flux, and $\Delta\Pi_{avg}$ is the average osmotic pressure difference across the membrane, which can be approximated with the Carnahan and Starling corrected van't Hoff approximation [55], [56]:

Equation 3.7
$$\Pi = \frac{RT}{\overline{V_W}} \ln(a_w) \approx RT\left(\frac{1++\Psi^2-\Psi^3}{(1-\Psi)^3}\right)\sum_i C_i$$

where Ψ is the volume fraction of the solute in the solution and C_i is the molar concentration (mol/L).

3.2.3.5 Conservation of mass

Transportation of water and all the components at each computation grid is performed by mass balance. After convergence of concentrations and current density, the effluent to the next grid is computed with the following equation:

Equation 3.8
$$N_{w,n+1} = N_{w,n} - J_{electro-osmosis} w \Delta y$$

where $N_{w,n}$ is the influent flow rate of water entering the *n*th grid, $N_{w,n+1}$ is the influent molar flow rate of water to the *n+1* th grid, *w* is the width of the *n*th grid in the z dimension (Figure 3.1),

and Δy is the length of *n* th grid along the flow path. The transported water from the diluate stream is added to the adjacent concentrate stream.

3.2.4 Ion Transport Modeling

In this section, the modeling of the transport of ions through an electrodialysis stack is explained. Speciation of feed stream components were calculated according to the model described in Chapter 2. Hence, the model calls the speciation subroutine for each discrete location to calculate the concentration and transport number of each water quality component. The molar flux under ionic concentration gradient and electric field for a specific ion within the electrodialysis stack (in the x-direction) was approximated by the Nernst-Planck Equation:

Equation 3.9 $$J_i = -D_i \frac{dc_i}{dx} - \frac{\lambda_i c_i}{F} \frac{d\phi}{dx}$$

where for the i^{th} species, J_i is the molar flux, D_i is the ionic diffusivity, c_i is the molar concentration, F is the Faraday constant, ϕ is the electric potential, and λ_i is equivalent ionic conductivity that can be calculated as explained in Equation 2.16 and Equation 2.17 [14]. By adding the fluxes of charges, the electrical current density of the n^{th} grid is calculated as:

Equation 3.10 $$i_n = F \sum_i z_i J_{i,n}$$

Since the bulk region is approximated as well-mixed, the concentration gradient would be zero, and Equation 3.9 simplifies to Equation 3.11:

Equation 3.11 $$J_i = -\frac{\lambda_i c_i}{F} \frac{d\phi}{dx}$$ (bulk region only)

where the electric potential gradient in the bulk region is equal to:

Equation 3.12 $$\nabla \phi_{bulk} = -\frac{i}{\kappa}$$

The current density should be constant due to steady-state conservation of charges. Assuming constant concentration gradient within the boundary layer, the concentration gradient can be estimated as:

Equation 3.13
$$\frac{dc_i}{dx} = -\frac{1}{D_i}\left(J_i + \frac{\lambda_i c_i}{F}\frac{d\phi}{dx}\right)$$

where ∇c_i is the concentration gradient of species i.

As explained above, the DBL is controlled by hydrodynamic conditions; therefore, the concentration of each ion at the membrane surface is equal to:

Equation 3.14
$$c_{mem} = c_{i,bulk} + \frac{dc_i}{dx}\ \delta$$

3.2.5 Electrical Device Modeling

In this section, the modeling of an electrodialysis stack as an electrical device is described.

3.2.5.1 Current density

An electrodialysis stack can be modeled as an electrical resistor with current density of *i* (A/m^2):

Equation 3.15
$$i = \frac{\Delta\phi_{applied} - \Delta\phi_{electrodes} - \sum \Delta\phi_{stack\ losses}}{\tilde{R}_{ed}}$$

where $\sum \Delta\phi$ is the potential (voltage) loss through the stack (the membranes and solutions), and $\tilde{R}_{ed}$ is the area-specific electrical resistance ($\Omega\ m^2$) of the stack [57].

3.2.5.2 Voltage Losses inside the ED stack

The main voltage losses in a cell-pair within an electrodialysis stack include: (1) Ohmic voltage losses due to electrical resistance of membranes and bulk solutions, (2) liquid junction or "Donnan" potentials, and (3) diffusion potentials (described above).

3.2.5.2.1 Donnan potentials

An electrical voltage difference across the membranes is caused by a difference in salinity difference (different ion activities) across the membranes, and this voltage difference is called the liquid junction potential (or Donnan potential) [58], [59]. This voltage basically counteracts the applied voltage from the electrodes and can be significant. The general form of the calculation of the Donnan potential (assuming constant transport number across the membranes) is [59]:

Equation 3.16 $$\left|\Delta\phi_{jct}\right| = \frac{R_g T}{F}\sum_i \frac{t_i}{z_i} ln \frac{\alpha_i^{HC}}{\alpha_i^{LC}}$$

where α_i^{HC} and α_i^{LC} are ionic activity for high concentration (HC) and low concentration (LC) sides, respectively [14], subscript of i is the ith species, R_g is the gas constant (8.314 J.mol^{-1}.K^{-1}), T is the temperature (°F), F is Faraday constant (96,485 s.A.mol^{-1}), z the ionic charge, and t is the transport number (transference number) which is the fractional contribution of i^{th} ion to transport electrical current across the membrane and calculates as below:

Equation 3.17 $$t_i = \frac{|z_i|u_i C_i}{\sum|z_j|u_j C_j}$$

as it was discussed in the previous chapter, conductivity calculates as below:

Equation 3.18 $$\kappa = F\sum|z_i|u_i C_i$$

3.2.5.2.2 Diffusion boundary layer potential gradient

The potential gradient of the diffusion boundary layer (DBL) calculates as:

Equation 3.19 $$\nabla\phi_{DBL} = -\frac{i}{\kappa} + \nabla\phi_{diff}$$

where $\nabla\phi_{diff}$ is the diffusion potential, which is an electrical potential gradient formed by salinity gradient and various diffusivities of its ions. This occurs to maintain electroneutrality in each DBL and is calculated as:

Equation 3.20

$$\nabla\phi_{diff} = -\frac{R_g T}{F\kappa} + \sum_i \lambda_i \nabla c_i$$

3.2.5.2.3 Electrical resistance within the stack

The area-specific resistance of a cell-pair, $\tilde{R}_{cp}$, can be estimated as the sum of membranes (CEMs, subscript *c*, and AEMs, subscript *a*) and the solutions surrounding them, including concentrate (subscript *C*) and diluate (subscript *D*) bulk and diffusion boundary layers (subscript *bl*) as follows:

Equation 3.21

$$\tilde{R}_{cp} = \tilde{R}_{CEM} + \tilde{R}_{c,DBL-c} + \tilde{R}_{c,bulk} + \tilde{R}_{c,DBL-a} + \ldots$$
$$\ldots + \tilde{R}_{AEM} + \tilde{R}_{d,DBL-a} + \tilde{R}_{d,bulk} + \tilde{R}_{d,DBL-c}$$

The total resistance of an electrodialysis stack is simply the product of the total number of cell pairs and resistance of a cell pair:

Equation 3.22

$$\tilde{R}_{ed} = N_{cp}\tilde{R}_{cp}$$

3.3 Results and discussions

A steady-state electrodialysis model for ED was developed to consider the hydraulic, chemical, and electrical reactions that occur in the electrodialysis stack. This model calculates the electrical current density, ion transport, water transport, and resulting compositions for concentrate and diluate streams at 18 discrete points along the flow path inside the ED stack. The model executed within 6 s with an Intel® Core™ i7-8650U CPU @ 1.9 GHz processor. The results for a feed solution with real brackish water solution with conductivity of 5.1 mS/cm and two flow rates of 5 cm/s and 13 cm/s is compared with the triplicate performed experiments for each flow velocities and varying voltage settings. The comparison of model predictions and measured current densities showed reasonable accuracy with relative root mean square error (RRMSE) of 11% for low and high velocities, as it is shown in Figure 3.3.

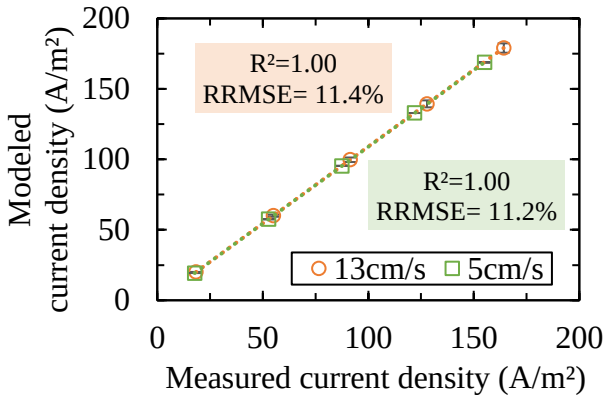

Figure 3.3: Comparison of modeled and measured current density throughout the experiments (n=3) for varying velocities

A comparison of modeled and measured relative conductivity of concentrate and feed streams is shown in Figure 3.4 (a). The model prediction of outlet conductivity is correlated very well with experimentally measured values (R^2>0.98) for low and high superficial velocities. The corresponding conductivity reduction is shown in Figure 3.4 (b) and RRMSE of the model was of 13% and 19% for 5 cm/s and 13 cm/s, respectively.

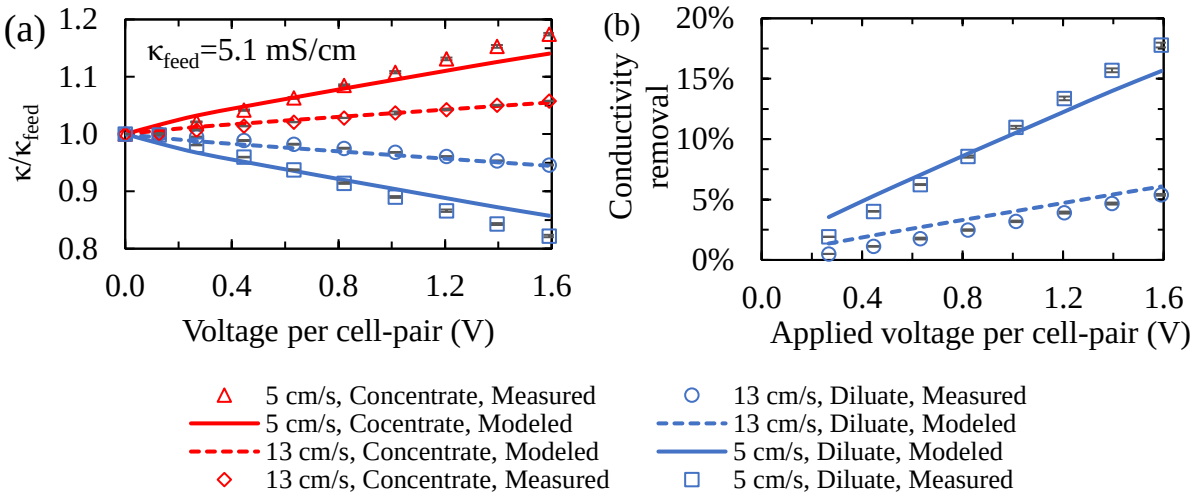

Figure 3.4: (a) Comparison of modeled and measured relative conductivity (n=3) for diluate and concentrate outlets at different currents, flow velocities, for feed concentrations of 5.1 mS/cm, (b) comparison of conductivity removal for flow velocities of 5 cm/s and 13 cm/s

Modeled and measured relative concentration for concentrate and diluate outlets are shown in Figure 3.5 for (a) sodium, (b) chloride, (c) calcium, and (d) sulfate, respectively. Model

predictions for sodium and chloride were fairly consistent (R^2>0.96) with RRMSE values under 12%, but the model significantly underpredicted calcium separation and overpredicted sulfate separation (However, the model does not account for ion selective membranes such as the monovalent anion exchange membranes used in the experimentation).

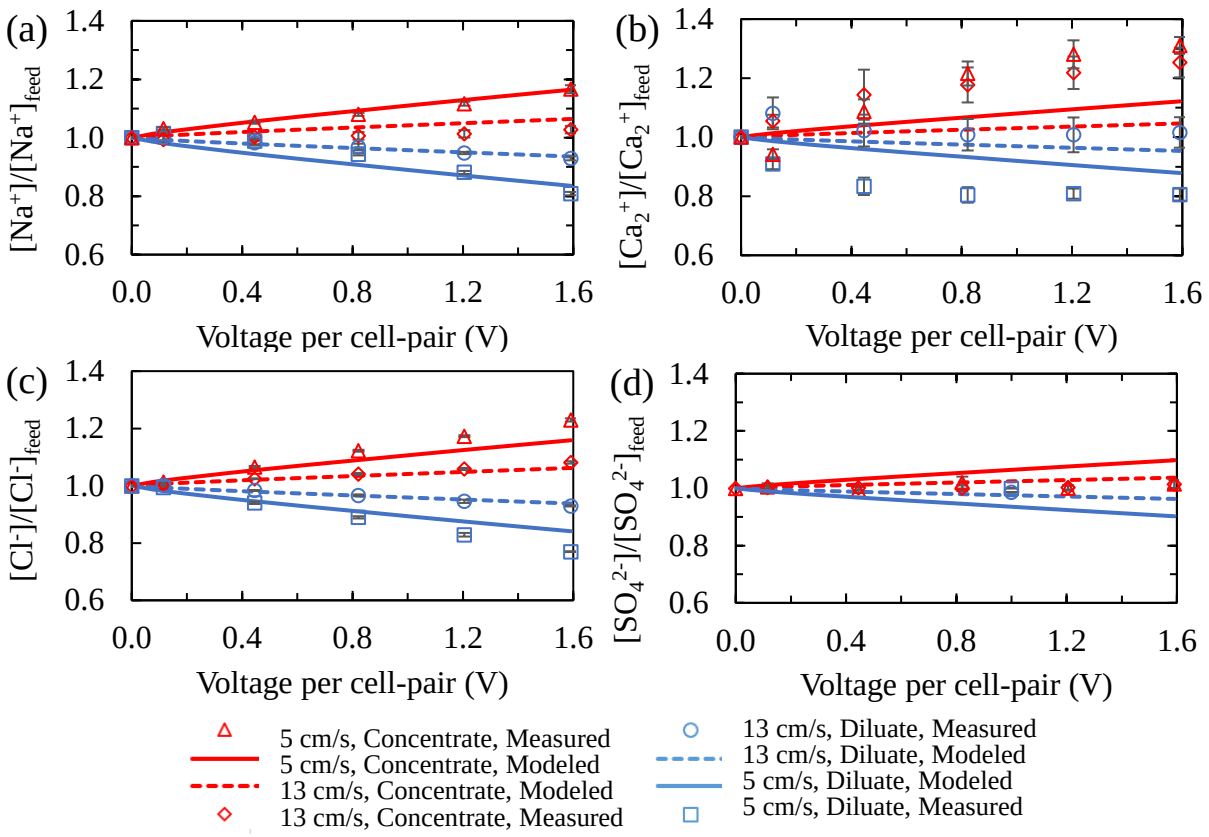

Figure 3.5: Comparison of modeled and measured (n=3) relative concentrations for diluate and concentrate outlets at different voltage, flow velocity, in feed solution of 5.1 mS/cm for: (a) Sodium, (b) Calcium, (c) Chloride, and (d) Sulfate, respectively

The model predictions for sodium and chloride removal were highly correlated (R^2>0.98) (Figure 3.6 (a) and (c)), while is not as accurate for calcium and sulfate (Figure 3.6 (b) and (d)).

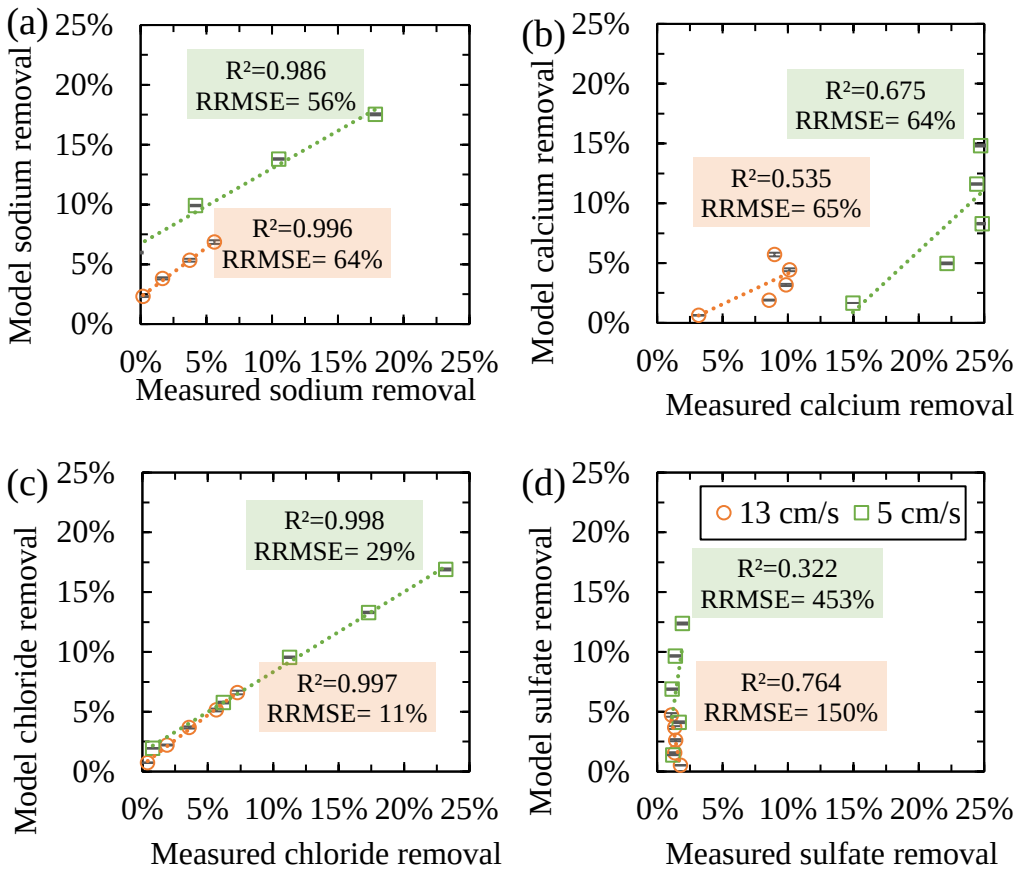

Figure 3.6: Comparison of modeled and measured concentration reduction (n=3) at different voltage, flow velocity, in feed solution of 5.1 mS/cm for: (a) Sodium, (b) Calcium, (c) Chloride, and (d) Sulfate, respectively

The model prediction of SEC was highly correlated with the measured SEC values (R^2>0.99), with RRMSE of 8% and 18% for low and high velocities, respectively, as it is shown in Figure 3.7 (a). To achieve conductivity removal of 18% and 5%, SEC of 0.41 kWh/m^3 and 0.14 kWh/m^3 was needed for low and high velocities, respectively. The normalized SEC was predicted higher in 5 cm/s compared to 13 cm/s with RRMSE of 24% and 16%, respectively, as it is shown in Figure 3.7 (b).

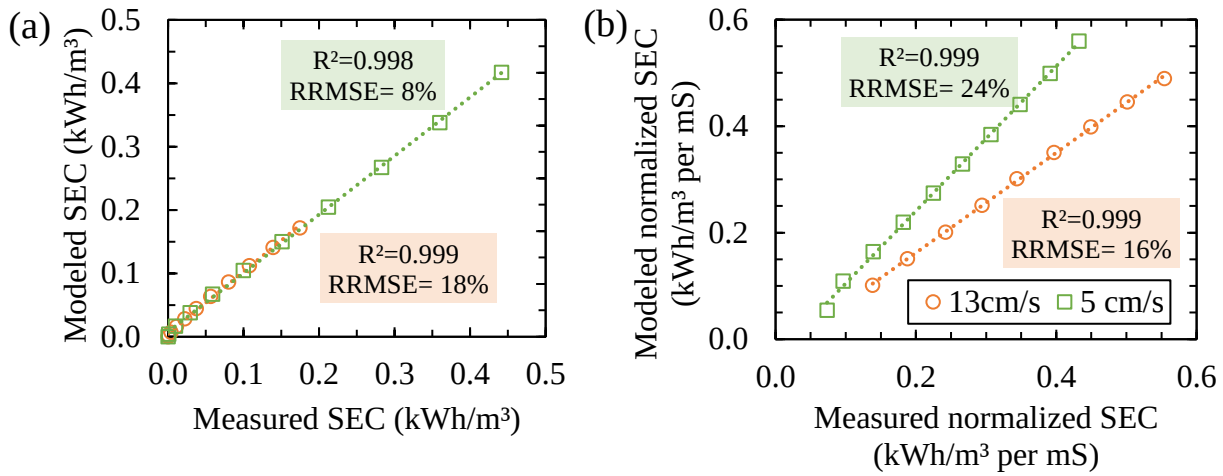

Figure 3.7: Comparison of modeled and measured (a) SEC, (b) normalized SEC

3.4 Conclusions

A novel theoretical model was developed to predict brackish water desalination with electrodialysis (ED). The main advantage of this model compared to other models is the Nernst-Planck simulation of multicomponent ionic transport that is computationally efficient compared to more complex models. The model was compared to experimental data at multiple velocities and voltages, which showed precise modeling results for current density, overall conductivity, and separation of sodium and chloride.

The model predicted the current densities of flow velocities of 5 cm/s and 13 cm/s with R^2 of 1.00 and 1.00 and RRMSE of 11.2% and 11.4%, respectively. The conductivity reduction prediction was more accurate at a lower flow velocity with R^2 of 0.9998 and RRMSE of 13%, compare to R^2 of 0.9997 and RRMSE of 19% for higher flow velocity. The model was not able to predict the concentration reduction of calcium and sulfate accurately, most likely because the model does not account for membrane selectivity. The SEC prediction for low and high velocity was precisely predicted with RRMSE values of 8% and 18%, respectively.

Future work should include incorporating membrane selectivity into the ion transport modeling, as well as modeling electrodialysis treatment of RO concentrate waste. Adding temperature functions and solubility factors can be helpful for more accurate modeling predictions.

General Conclusions

This research was focused on operation and theoretical modeling of electrodialysis (ED) desalination of real multicomponent brackish water based on multi-component solutions. The significance of this work was to advance modeling tools for the desalination industry that can be applied to specific water quality and membrane properties. The developed electrical conductivity model is generally applicable to a wide range of salinity, and the developed steady-state electrodialysis model is customizable based on different characteristics of desalination process such as water quality, membrane properties, stack dimensions, flow velocities, and applied voltage. The electrodialysis model was validated with several experiments with a real brackish water feed source to show the capabilities and accuracy of the developed model. Not only does this model provide a more thorough and realistic understanding of the ED process, but this also enables other researchers to have an accurate estimation of the system performance based on the properties of their system and source feed water.

Future development of this model is expected to have promising results as the model is validated for a wide range of multi-component solutions and other membranes and spacers. The future studies can use the same developed modeling platform to test the effects of various water quality parameters and feed sources (*e.g.*, more concentrated solution such as RO reject) to predict the performance of the ED process. Adding membrane selectivity capabilities to the model based on transport numbers will further improve the robustness and general applicability of the model.

Finding the optimal tradeoffs between salt removal and energy consumption is possible using this model, which will generally lead to more affordable produced water. Furthermore, providing an open source model for researchers as well as operators can help avoid trial and error efforts in optimization of ED. This is a promising enhancement for water treatment industry to

make a more accessible pure water for everyone by making a more efficient and competitive technology.

Appendix A

Water Ionic Product

The ionic product of water (K_W) is production of activities of hydrogen and hydroxide ions. This parameter is a function of temperature and density of water while the latter is also dependent on temperature. It is equal to 10^{-14} for water at 25°C. However, in order to compute it more precisely for a wide range of temperatures, the *Equation B.1* has been used [60]:

Equation B.1 $$log_{10}K_w^* = c_1 + \frac{c_2}{T} + \frac{c_3}{T^2} + \frac{c_4}{T^3} + (c_5 + \frac{c_6}{T} + \frac{c_7}{T^2}) \times log_{10}\rho_w^*$$

Where $K_w^* = \frac{K_W}{(\frac{mol}{kg})}$, and $\rho_w^* = \frac{\rho_W}{(\frac{g}{cm^3})}$, to make water ionic product and density normalized by their units. The parameters in *Equation B* are:

$c_1 = -4.098$, $c_2 = -3245.2\text{K}$, $c_3 = 2.2362 \times 10^5\text{K}^2$, $c_4 = -3.984 \times 10^7\text{K}^3$, $c_5 = 13.957$, $c_6 = 1262.3\text{K}$, $c_7 = 8.5641 \times 10^5\text{K}^5$, T= Temperature (K) [60]

To calculate the density of water $\rho_w \left(\frac{g}{cm^3}\right)$, the Equation B.2 which is obtained from empirical experiences for pure water has been used [61]:

Equation B.2 $$\rho_w(T) = 0.99985 + 6.32693 \times 10^{-5}T - 8.52829 \times 10^{-6}T^2 + 6.94325 \times 10^{-8}T^3 - 3.82122 \times 10^{-7}T^4$$

As shown in Figure B, the interpolation of water density for temperatures between 0 to 100 °C has a R^2=0.999 (CRC).

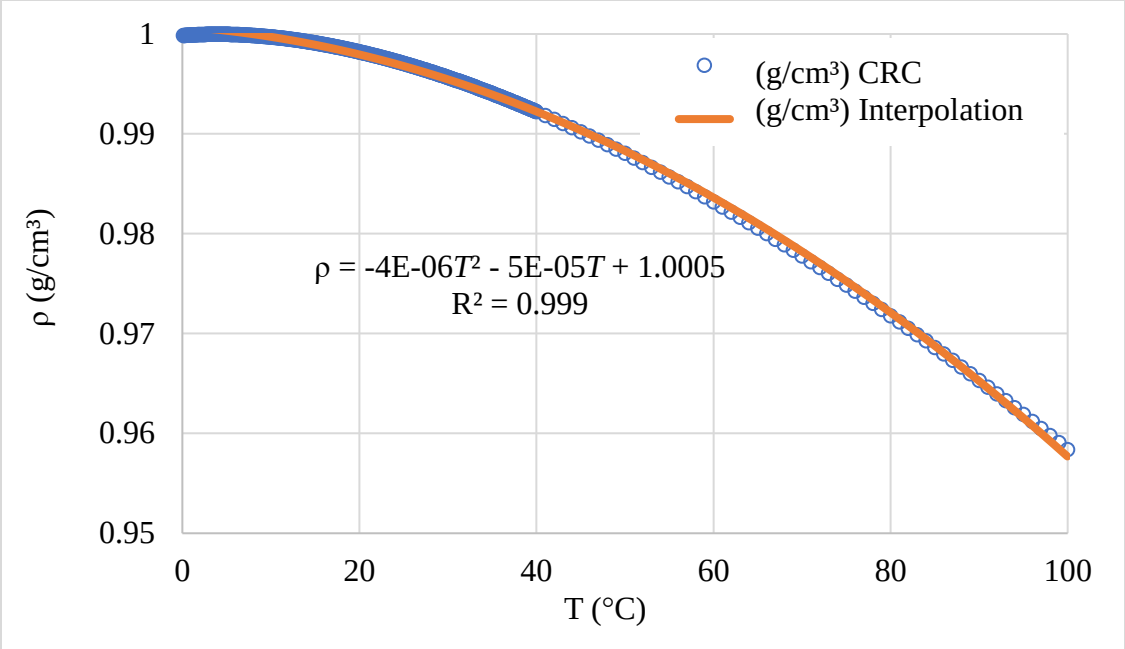

Figure B.1: Interpolation of water density as a function of temperature [62]

Where t is temperature (°C). The precision of the interpolated water density is in the order of 0.1% for temperatures in the range of 0 to 60ºC.

References

[1] S. H. Schneider and F. K. Hare, *Encyclopedia of climate and weather*, vol. 678. Oxford university press New York, 1996.

[2] L. F. Greenlee, D. F. Lawler, B. D. Freeman, B. Marrot, and P. Moulin, "Reverse osmosis desalination: water sources, technology, and today's challenges," *Water Res.*, vol. 43, no. 9, pp. 2317–2348, 2009.

[3] A. Campione, L. Gurreri, M. Ciofalo, G. Micale, A. Tamburini, and A. Cipollina, "Electrodialysis for water desalination: A critical assessment of recent developments on process fundamentals, models and applications," *Desalination*, vol. 434, no. October 2017, pp. 121–160, 2018, doi: 10.1016/j.desal.2017.12.044.

[4] J. Luh and B. J. Mariñas, "Kinetics of bromochloramine formation and decomposition," *Environ. Sci. Technol.*, vol. 48, no. 5, pp. 2843–2852, 2014, doi: 10.1021/es4036754.

[5] L. M. Camacho, J. A. Fox, and J. O. Ajedegba, "Optimization of electrodialysis metathesis (EDM) desalination using factorial design methodology," *Desalination*, vol. 403, pp. 136–143, 2017.

[6] V. Sarapulova *et al.*, "Transport characteristics of fujifilm ion-exchange membranes as compared to homogeneous membranes AMX and CMX and to heterogeneous membranes MK-40 and MA-41," *Membranes (Basel).*, vol. 9, no. 7, pp. 1–23, 2019, doi: 10.3390/membranes9070084.

[7] E. Y. Safronova *et al.*, "New cation-exchange membranes based on cross-linked sulfonated polystyrene and polyethylene for power generation systems," *J. Memb. Sci.*, vol. 515, pp. 196–203, 2016.

[8] H. Garmes, F. Persin, J. Sandeaux, G. Pourcelly, and M. Mountadar, "Defluoridation of

groundwater by a hybrid process combining adsorption and Donnan dialysis," *Desalination*, vol. 145, no. 1–3, pp. 287–291, 2002, doi: 10.1016/S0011-9164(02)00424-1.

[9] Y. Sedkaoui, A. Szymczyk, H. Lounici, and O. Arous, "A new lateral method for characterizing the electrical conductivity of ion-exchange membranes," *J. Memb. Sci.*, vol. 507, pp. 34–42, 2016.

[10] J. Moreno, S. Grasman, R. Van Engelen, and K. Nijmeijer, "Upscaling Reverse Electrodialysis," *Environ. Sci. Technol.*, vol. 52, no. 18, pp. 10856–10863, 2018, doi: 10.1021/acs.est.8b01886.

[11] E. J. Calvo, "Electrochemical methods for sustainable recovery of lithium from natural brines and battery recycling," *Curr. Opin. Electrochem.*, vol. 15, pp. 102–108, 2019.

[12] J. Veerman, "The effect of the NaCl bulk concentration on the resistance of ion exchange membranes-measuring and modeling," *Energies*, vol. 13, no. 8, 2020, doi: 10.3390/en13081946.

[13] Y. Kim, W. S. Walker, and D. F. Lawler, "Electrodialysis with spacers: Effects of variation and correlation of boundary layer thickness," *Desalination*, vol. 274, no. 1–3, pp. 54–63, 2011.

[14] A. J. Bard and L. R. Faulkner, "Fundamentals and applications," *Electrochem. Methods*, vol. 2, p. 482, 2001.

[15] W. S. Walker, "Improving recovery in reverse osmosis desalination of inland brackish groundwaters via electrodialysis," pp. 1–211, 2010.

[16] M. Ben Sik Ali, A. Mnif, B. Hamrouni, and M. Dhahbi, "Electrodialytic desalination of brackish water: Effect of process parameters and water characteristics," *Ionics (Kiel).*, vol.

16, no. 7, pp. 621–629, 2010, doi: 10.1007/s11581-010-0441-2.

[17] C. Han and T. Yan, “Mathematical modeling for desalination by electrodialysis,” *Res. J. Chem. Environ.*, vol. 15, no. 2, pp. 39–43, 2011, doi: 10.1016/j.desal.2006.04.062.

[18] R. W. Baker, “Overview of membrane science and technology,” *Membr. Technol. Appl.*, vol. 3, pp. 1–14, 2004.

[19] Y. Tanaka, “Current density distribution, limiting current density and saturation current density in an ion-exchange membrane electrodialyzer,” *J. Memb. Sci.*, vol. 210, no. 1, pp. 65–75, 2002.

[20] R. B. McCleskey, D. K. Nordstrom, J. N. Ryan, and J. W. Ball, “A new method of calculating electrical conductivity with applications to natural waters,” *Geochim. Cosmochim. Acta*, vol. 77, pp. 369–382, 2012, doi: 10.1016/j.gca.2011.10.031.

[21] E. W. Rice, R. B. Baird, A. D. Eaton, and L. S. Clesceri, *Standard methods for the examination of water and wastewater*. 2017.

[22] D. K. Nordstrom, J. W. Ball, and D. I. N. Biogeochemistry, *Complexation of trace metals in natural waters*. Dordrecht: Springer Netherlands, 1984.

[23] G. Tick and D. Vlassopoulos, “AqQA: quality assurance and presentation graphics for ground water analyses,” *Ground Water*, vol. 42, no. 3, pp. 326–329, 2004.

[24] D. L. Parkhurst and C. A. J. Appelo, “Description of Input and Examples for PHREEQC Version 3 — A Computer Program for Speciation , Batch-Reaction , One-Dimensional Transport , and Inverse Geochemical Calculations. U.S. Geological Survey Techniques and Methods, book 6, chapter A43, 497 p.,” *U.S. Geol. Surv. Tech. Methods, B. 6, chapter A43*, pp. 6-43A, 2013, doi: 10.1016/0029-6554(94)90020-5.

[25] M. E. Wieser *et al.*, “Atomic weights of the elements 2011 (IUPAC Technical Report),”

Pure Appl. Chem., vol. 85, no. 5, pp. 1047–1078, 2013.

[26] W. Stumm, J. J. Morgan, and Stumm, *Aquatic chemistry: chemical equilibria and rates in natural waters*, vol. 126. John Wiley & Sons, 2012.

[27] D. R. Lide, *Ionic conductivity and diffusion at infinite dilution*. 2005.

[28] J. P. Gustafsson, "Visual MINTEQ 3.1 user guide," *Dep. L. Water Resour. Eng. R. Inst. Technol. Stokholm, Sweden*, pp. 1–73, 2014.

[29] J. W. Ball and D. K. Nordstrom, "USER'S MANUAL FOR WATEO4F, WTTH REVISED THERMODYNAMIC DATA BASE AND TEST CASES FOR CALCULATING SPECIATION OF MAJOR, TRACE, AND REDOX ELEMENTS IN NATURAL WATERS," 1991.

[30] M. R. Wright, *An introduction to aqueous electrolyte solutions*. John Wiley & Sons, 2007.

[31] C. G. Malmberg and A. A. Maryott, "Dielectric Constant of Water from 0 to 100 C," *J. Res. Nat. Bur. Stand*, vol. 56, pp. 369131–369138, 1956.

[32] C. N. Sawyer, P. L. McCarty, and G. F. Parkin, "Chemistry for environmental engineering and science," 2003.

[33] J. P. Gustafsson, "Visual MINTEQ ver. 3.1," *Dep. L. Water Resour. Eng. R. Inst. Technol. Stokholm, Sweden*, 2014.

[34] "Chemical Entities of Biological Interest (ChEBI). UK," *European Bioinformatics Institute*, 2017. .

[35] K. S. Johnson, "Carbon dioxide hydration and dehydration kinetics in seawater," *Limonology Oceanogr.*, vol. 27, no. 5, pp. 849–855, 1982, doi: 10.4319/lo.1982.27.5.0849.

[36] J. F. Kerrisk, "Chemical-equilibrium calculations for aqueous geothermal brines," Los

Alamos National Lab., NM (USA), 1981.

[37] G. Kortüm, “Treatise on electrochemistry,” 1965.

[38] H. J. Lee, F. Sarfert, H. Strathmann, and S. H. Moon, “Designing of an electrodialysis desalination plant,” *Desalination*, vol. 142, no. 3, pp. 267–286, 2002, doi: 10.1016/S0011-9164(02)00208-4.

[39] M. T. Myint and A. Ghassemi, “Electrodialysis reversal desalination: Monographs for the design parameters,” *Desalin. Water Treat.*, vol. 48, no. 1–3, pp. 106–119, 2012, doi: 10.1080/19443994.2012.698802.

[40] L. Karimi, L. Abkar, M. Aghajani, and A. Ghassemi, “Technical feasibility comparison of off-grid PV-EDR and PV-RO desalination systems via their energy consumption,” *Sep. Purif. Technol.*, vol. 151, pp. 82–94, 2015, doi: 10.1016/j.seppur.2015.07.023.

[41] C. Hanrahan, L. Karimi, A. Ghassemi, and A. Sharbat, “High-recovery electrodialysis reversal for the desalination of inland brackish waters,” *Desalin. Water Treat.*, vol. 57, no. 24, pp. 11029–11039, 2016, doi: 10.1080/19443994.2015.1041162.

[42] L. Karimi, A. Ghassemi, and H. Zamani Sabzi, “Quantitative studies of electrodialysis performance,” *Desalination*, vol. 445, no. July, pp. 159–169, 2018, doi: 10.1016/j.desal.2018.07.034.

[43] M. Sadrzadeh, A. Kaviani, and T. Mohammadi, “Mathematical modeling of desalination by electrodialysis,” *Desalination*, vol. 206, no. 1–3, pp. 538–546, 2007, doi: 10.1016/j.desal.2006.04.062.

[44] M. Thein, A. Ghassemi, and N. Nirmalakhandan, “Modeling in desalination — electro-dialysis reversal,” vol. 27, pp. 255–267, 2011.

[45] V. Nikonenko, A. Nebavsky, S. Mareev, A. Kovalenko, M. Urtenov, and G. Pourcelly,

"Modelling of Ion Transport in Electromembrane Systems: Impacts of Membrane Bulk and Surface Heterogeneity," *Appl. Sci.*, vol. 9, no. 1, p. 25, 2018, doi: 10.3390/app9010025.

[46] A. Campione *et al.*, "A hierarchical model for novel schemes of electrodialysis desalination," *Desalination*, vol. 465, no. July 2018, pp. 79–93, 2019, doi: 10.1016/j.desal.2019.04.020.

[47] M. M. Benjamin and D. F. Lawler, *Water quality engineering: Physical/chemical treatment processes*, vol. 111, no. 479. John Wiley & Sons, 2013.

[48] H. J. Lee, F. Sarfert, H. Strathmann, and S. H. Moon, "Designing of an electrodialysis desalination plant," *Desalination*, 2002, doi: 10.1016/S0011-9164(02)00208-4.

[49] K. M. Chehayeb and K. G. Nayar, "On the merits of using multi-stage and counterflow electrodialysis for reduced energy consumption," *Desalination*, vol. 439, pp. 1–16, 2018.

[50] K. M. Chehayeb, D. M. Farhat, and K. G. Nayar, "Optimal design and operation of electrodialysis for brackish-water desalination and for high-salinity brine concentration," *Desalination*, vol. 420, pp. 167–182, 2017.

[51] K. M. Chehayeb, "Entropy generation analysis of electrodialysis," *Desalination*, vol. 413, pp. 184–198, 2017.

[52] E. L. Cussler, *Diffusion: mass transfer in fluid systems*. Cambridge university press, 2009.

[53] C. C. John, J. C. Crittenden, R. R. Trussell, D. W. Hand, K. J. Howe, and G. Tchobanoglous, *MWH's water treatment: principles and design*. John Wiley & Sons, 2012.

[54] J. O. Bockris and A. K. N. Reddy, "Modern Electrochemistry, Vol. 1," *Macdonald, London*, vol. 2, 1998.

[55] M. M. Benjamin and D. F. Lawler, *Water quality engineering: Physical/chemical treatment processes*. John Wiley & Sons, 2013.

[56] W. S. Walker, Y. Kim, and D. F. Lawler, "Treatment of model inland brackish groundwater reverse osmosis concentrate with electrodialysis — Part II: Sensitivity to voltage application and membranes," *Desalination*, vol. 345, pp. 128–135, 2014, doi: 10.1016/j.desal.2014.04.026.

[57] F. Valero and R. Arbós, "Desalination of brackish river water using Electrodialysis Reversal (EDR): control of the THMs formation in the Barcelona (NE Spain) area," *Desalination*, vol. 253, no. 1–3, pp. 170–174, 2010.

[58] P. Henderson, "Zur thermodynamik der flüssigkeitsketten," *Zeitschrift für Phys. Chemie*, vol. 59, no. 1, pp. 118–127, 1907.

[59] W. Huang, W. S. Walker, and Y. Kim, "Junction potentials in thermolytic reverse electrodialysis," *Desalination*, vol. 369, pp. 149–155, 2015, doi: 10.1016/j.desal.2015.05.005.

[60] D. R. D. (Ed) Lide, *Ion product of water substance*. 2010.

[61] F. E. Jones and G. L. Harris, "ITS-90 density of water formulation for volumetric standards calibration.," *J. Res. Natl. Inst. Stand. Technol.*, vol. 97, no. 3, pp. 335–340, 1992.

[62] D. R. Lide, *CRC handbook of chemistry and physics*, vol. 85. CRC press, 2004.

Curriculum Vita

Shahrouz Jafarzade Ghadimi obtained his Bachelor of Engineering degree in Civil Engineering at the Iran University of Science and Technology, Tehran, Iran in 2013. He obtained his Master of Science degree in Environmental Engineering in 2015. His PhD research work was funded by the National Science Foundation (NSF) and supported by the Nanosystems Engineering Research Center for Nanotechnology-Enabled Water Treatment (NEWT). His research includes experimental testing and mathematical modeling of electrodialysis desalination. Shahrouz also gained relevant experience operating a commercial electrodialysis reversal pilot at the Brackish Groundwater National Desalination Research Facility (BGNDRF), Alamogordo, NM. Additionally, he participated in an industrial internship with Carollo Engineers consulting firm in Phoenix, AZ to assist the development team for Blue Plan-it® (a water industry decision-making software). Eventually, Shahrouz's hope is to help people access more affordable water by working in industry.

Contact Information: <sjghadimi@hotamil.com>

Web: www.linkedin.com/in/sjghadimi